JOURNAL OF PETROLOGY | VOLUME 45 | NUMBER 00 | PAGES 1–22 | 2003 | DOI: 10.1093/petrology/egg107

Silicate, Hydrous and Carbonate Metasomatism at Lherz, France: Contemporaneous Derivatives of Silicate Melt–Harzburgite Reaction

JEAN-LOUIS BODINIER[1]*, MARTIN A. MENZIES[2], NOBUMICHI SHIMIZU[3], FREDERICK A. FREY[4] AND ELAINE McPHERSON[2]

[1]LABORATOIRE DE TECTONOPHYSIQUE, ISTEEM, CASE 49, CNRS ET UNIVERSITÉ DE MONTPELLIER 2, PLACE EUGÈNE BATAILLON, 34095 MONTPELLIER CEDEX 05, FRANCE

[2]DEPARTMENT OF GEOLOGY, ROYAL HOLLOWAY, UNIVERSITY OF LONDON, EGHAM HILL, EGHAM TW20 0EX, UK

[3]DEPARTMENT OF GEOLOGY AND GEOPHYSICS, WOODS HOLE OCEANOGRAPHIC INSTITUTION, WOODS HOLE, MA 02543, USA

[4]DEPARTMENT OF EARTH, ATMOSPHERIC AND PLANETARY SCIENCES, MASSACHUSETTS INSTITUTE OF TECHNOLOGY, CAMBRIDGE, MA 02139, USA

RECEIVED NOVEMBER 18, 2002; ACCEPTED SEPTEMBER 5, 2003

Complex multi-stage models involving silicate, hydrous and carbonate melts of distinct provenance have been invoked to explain the metasomatism observed in mantle rocks. In contrast, relatively simple models requiring polybaric crystallization of alkaline silicate melts have been proposed to explain the occurrence of veined mantle rocks. To address the spatial and temporal relationships between veins and wall-rocks, a sequence of drill cores was obtained from Lherz, France. In outcrop the vein (amphibole–garnet pyroxenite dyke) is spatially associated with hornblendite veinlets (lherzite), and proximal amphibole-bearing and distal apatite-bearing wall-rock peridotite. Considerable elemental and isotopic heterogeneity exists in these wall-rock peridotites, in many instances equivalent to, or greater than, that observed in mantle xenoliths from worldwide localities. A single stage of reactive porous flow best explains the elemental and isotopic heterogeneity in the wall-rock. In essence it is proposed that emplacement of the silicate melt (dyke) was inextricably linked to chromatographic fractionation/reaction of derivatives which led to the coexistence, in space and time, of silicate, hydrous and carbonate melts. This model elegantly and simply describes the formation of complex metasomatic aureoles around mantle veins and negates the need, in the case of basalt-hosted (and kimberlite-hosted) xenoliths, for complex multi-stage models involving several episodes of melt influx with each melt being of different provenance.

KEY WORDS: *mantle metasomatism; trace-element enrichment; isotopic contamination; wall-rock peridotite; Lherz peridotite*

INTRODUCTION AND AIMS

The Lherz massif, Etang de Lers in the French Pyrenees, is the type locality for lherzolite first described by Le Lievre in 1787, who noted the olivine-rich character of the massif and the similarity to peridotite xenoliths entrained in volcanic rocks in the Massif Central. De La Metherie coined the term 'lherzolite'. Over 200 years later orogenic peridotites, and especially the Lherz massif, are pivotal to our understanding of the temporal and spatial aspects of melt transfer through mantle rocks. This massif has been the focus of many studies of melt transfer processes within mantle rocks and in recent years has been the source of debate concerning mantle processes (Polvé & Allègre, 1980; Wilshire *et al.*, 1980; Loubet & Allègre, 1982; Bodinier *et al.*, 1987*a*, 1987*b*, 1988, 1990; Hamelin & Allègre, 1988; Vétil *et al.*, 1988; Downes *et al.*, 1991; Fabriès *et al.*, 1991; Mukasa *et al.*, 1991; Nielson & Wilshire, 1993; McPherson *et al.*, 1996; Pattou *et al.*, 1996;

*Corresponding author. E-mail: bodinier@dstu.univ-montp2.fr

Woodland *et al.*, 1996; Zanetti *et al.*, 1996; Lorand *et al.*, 1999).

In the Lherz orogenic peridotite, Bodinier *et al.* (1990) studied a 65 cm section of harzburgite wall-rock perpendicular to an amphibole–garnet pyroxenite dyke. Their results revealed significant mineralogical and chemical zonation of the wall-rock. At less than ~25 cm from the dyke–wall-rock boundary, hydrous amphibole-bearing peridotite displays patterns of decreasing concentrations of Fe, Ti, Mn, Al, Ca, Na and heavy rare earth elements (HREE), and increasing concentrations of Mg and Ni away from the dyke. In this zone, the chondrite-normalized REE patterns are convex-upward (0–15 cm) or U-shaped (15–25 cm) and relatively unfractionated (La_N/Yb_N ~1). At >25 cm from the dyke, anhydrous harzburgite displays a selective light REE (LREE) enrichment and Woodland *et al.* (1996) noted the presence of apatite in this zone. The normalized REE patterns vary from U-shaped at 25–30 cm (La_N/Yb_N ~1·7–2·6) to strongly LREE-enriched at 30–65 cm (La_N/Yb_N ~3–16). This variation encompasses almost the whole range of LREE/HREE ratios in metasomatized mantle xenoliths from alkali basalts. Bodinier *et al.* (1990) explained wall-rock zonation as a single-stage process involving progressive chemical evolution of melts infiltrated from the dyke into the harzburgite wall-rock. In this model, the compatible and moderately incompatible elements are buffered by the wall-rock peridotite proximal to the dyke (<20 cm) whereas distal to the dyke the most incompatible elements remain controlled by the infiltrated melt. This mechanism results in a chromatographic fractionation of REE and accounts for the high LREE/HREE ratios observed distal to the dyke (see also Zanetti *et al.*, 1996).

However, Nielson & Wilshire (1993) criticized this interpretation. In particular, they questioned the ability of mantle melts to percolate through lithospheric peridotites over distances greater than a few centimetres. This negated the very existence of chromatographic fronts in the upper mantle (Navon & Stolper, 1987). They suggested an interpretation for the Lherz wall-rock that involved multi-stage metasomatism with a requirement for vein conduits not seen in the peridotite block. At first sight, this interpretation appears to be supported by the isotopic data of Downes *et al.* (1991) in three samples from the Lherz wall-rock. These data indicate that the isotopic signature of the dyke does not extend over more than 20 cm into the wall-rock; yet the strong LREE enrichment typical of the host peridotite at >25 cm from the dyke has never been observed in peridotites unrelated to amphibole pyroxenite dykes, neither in Lherz nor in other Pyrenean peridotites (Bodinier *et al.*, 1988; McPherson *et al.*, 1996; Burnham *et al.*, 1998; Fabriès *et al.*, 1998). On the other hand, a similar composition has been found in harzburgites from the small Montau massif (western Pyrenees), which contain abundant and massive (metres thick) amphibole–feldspar segregates (J.-L. Bodinier, unpublished data, 2003).

To address some of these issues and the conflicting views, a new section was drilled in the Lherz wall-rock studied by Bodinier *et al.* (1990). Woodland *et al.* (1996) reported on the petrology and oxygen fugacity of these samples. Herein we report on a comprehensive geochemical study using data from several sources including X-ray fluorescence (XRF), inductively coupled plasma mass spectrometry (ICP-MS), secondary ion mass spectrometry (SIMS) and thermal ionization mass spectrometry (TIMS).

We are particularly interested in addressing several questions, as follows.

(1) What process best explains the mineralogical and chemical variability in the section from the dyke to proximal amphibole-bearing and distal anhydrous, apatite-bearing peridotites?

(2) Are we dealing with single- or multi-stage processes, and were the processes synchronous in time and space?

(3) If trace-element enrichment occurred during a single stage, can we reproduce with modelling the ultra-enrichment of LREE within the anhydrous peridotite (distal to the dyke) while keeping the isotopic contamination from the dyke restricted to the amphibole peridotite (proximal to the dyke)?

WALL-ROCK DESCRIPTION AND SAMPLING

The studied wall-rock is from a block of harzburgite that contains a dyke of amphibole–garnet pyroxenite, about 15 cm thick, and a complex swarm of bifurcating and anastomosing veins of 'lherzite' (= hornblendite). The lherzites are restricted to the wall-rock proximal to the main dyke (<25 cm). From this distance to the edge of the block (~80 cm from the dyke–wall-rock boundary), the harzburgite is devoid of dykes or veins (Woodland *et al.*, 1996, fig. 1). The dyke and veins cross-cut the harzburgite at a high angle to the foliation. They belong to a suite of hydrous pyroxenites considered as high-pressure–high-temperature crystal segregates from alkaline basalts that migrated through the Pyrenean lithospheric mantle in the Cretaceous (Loubet & Allègre, 1982; Goldberg *et al.*, 1986; Bodinier *et al.*, 1987*a*; Vétil *et al.*, 1988; Fabriès *et al.*, 1991; Rossy *et al.*, 1992). The conditions of emplacement of the dykes were estimated by Vétil *et al.* to be 1·0–1·5 GPa and 900–1000°C. Cross-cutting and overprinting relations indicate that the lherzite veins were emplaced at a slightly later stage than the pyroxenite dykes and were probably coeval with poikiloblastic amphibole developed at the expense of anhydrous primary minerals (pyroxene + garnet). The lherzites and the amphibole in the dykes are ascribed to the

segregation of volatile-rich, evolved melts after crystallization of anhydrous garnet pyroxenites from the alkaline basalt (Wilshire *et al.*, 1980; Bodinier *et al.*, 1988*a*; Woodland *et al.*, 1996).

Woodland *et al.* (1996) provided a detailed mineralogical description of the wall-rock samples collected for this study. The harzburgite wall-rock can be subdivided into two zones based upon textural, mineralogical and geochemical data: (1) an inner zone <25 cm from the main pyroxenite dyke and (2) an outer zone >25 cm from the main dyke (Bodinier *et al.*, 1990). This boundary is basically coincident with the most distant lherzite vein from the main dyke. The harzburgite in the inner zone has a well-developed porphyroclastic texture and contains disseminated brown amphibole and rare phlogopite, testifying to its modally metasomatized character. The amphiboles, sometimes replacing primary orthopyroxene, have compositions similar to those found in modally metasomatized spinel peridotite xenoliths (e.g. Menzies *et al.*, 1987). Several narrow (2–3 mm) irregularly bounded veinlets of amphibole and phlogopite occur sub-parallel to the lherzite veins in this zone. The outer zone, beyond the lherzite veins (>25 cm), has a granular to porphyroclastic texture and is essentially free of amphibole. The wall-rock in this zone appears to be texturally and mineralogically indistinguishable from 'normal' harzburgites from Lherz that are spatially unrelated to dykes. However, Woodland *et al.* (1996) identified rare grains of subhedral apatite in a number of samples from the outer zone, especially in the most distal part of the wall-rock (>50 cm from the dyke).

Twenty-five samples were drilled along a section perpendicular to the main dyke and veinlets, about 60 cm apart from the section studied by Bodinier *et al.* (1990). Among these samples, five were collected in the wall-rock of the main dyke opposite to that studied by Bodinier *et al.* (Woodland *et al.*, 1996, fig. 1). This wall-rock contains a subordinate amphibole–garnet pyroxenite dykelet and lherzite veins. It is comparable with the amphibole harzburgite zone defined in the main wall-rock with regard to texture, mineralogy and geochemistry (McPherson, 1994; Woodland *et al.*, 1996). These five samples will not be further considered in the present study. Among the other samples, two were drilled in the main dyke (samples EDL1, and 15), six are from the amphibole harzburgite wall-rock (<25 cm from the dyke: samples EDL17, 19, 20, 22, 24, and 27), among which sample EDL22 includes a lherzite veinlet, and 11 are from the distal harzburgite wall-rock (>25 cm: samples EDL28, 29, 30, 31, 32, 33, 35, 36, 37, 38 and 39).

ANALYTICAL METHODS

The samples were analysed as bulk rocks by XRF for major and several trace elements using the University of London XRF facility at Royal Holloway (RHUL). In addition, Rb, Sr, Y, Zr, Nb, Ba and Y were determined by quadrupole ICP-MS in selected samples at the NERC ICP-MS facility, RHUL. REE (La, Ce, Nd, Sm, Eu, Gd, Dy, Er, Yb and Lu) were determined by isotope dilution after separation, following the method of Thirlwall (1982) modified for the VG354 multicollector mass spectrometer of the radiogenic isotope laboratory at RHUL. Sr and Nd isotopes were also run on bulk rocks as it was impossible to separate sufficient clinopyroxene from the harzburgite cores, because of the small sample size. To remove secondary grain boundary components that may affect Sr isotopes, rock powders were leached in screwtop capsules at 180°C for 2 h in 6 M HCl. Confirmation that the leaching technique was effectively removing secondary minerals was sought by analysing fine sieve fractions from four xenoliths previously analysed using leached clinopyroxene (Downes *et al.*, 1992). It is also worth noting the consistency of our results with the Sr isotope data previously obtained by Downes *et al.* (1991) in three samples of leached clinopyroxene from the same wall-rock. These clinopyroxenes were separated from the whole-rock samples studied by Bodinier *et al.* (1990).

The isotope ratios were measured with multidynamic techniques (Thirlwall, 1991) on the VG354 at RHUL. Details of the analytical procedures have been given by McPherson *et al.* (1996), who also reported on the reproducibility and accuracy of trace-element and isotope analyses. Major-, trace-element and some Sr–Nd isotope data are given in Table 1 for 22 drilled cores.

In addition to the analyses performed in the new drilled section, a selection of 13 bulk-rock samples previously studied by Bodinier *et al.* (1990) were re-analysed for trace elements (Rb, Sr, Y, Zr, Nb, Cs, Ba, REE, Hf, Ta, Pb, Th and U) by ICP-MS at ISTEEM, University of Montpellier. We followed the procedures described by Ionov *et al.* (1992) and Godard *et al.* (2000), who reported the accuracy and reproducibility of the method based on repeated analyses of international peridotite standards. The results are given in Table 2.

Finally, clinopyroxenes and a few amphiboles from the main dyke and from 12 wall-rock samples were analysed in thin section by ion microprobe for Ti, V, Sr, Cr, Zr, Y and REE (La, Ce, Nd, Sm, Eu, Dy, Er and Yb). The analyses were performed by SIMS on a Cameca IMS 3f system at the Woods Hole Oceanographic Institution, following the procedure described by Shimizu & Hart (1982). Previous studies have reported reproducibility of clinopyroxene analyses obtained with this procedure (e.g. Takazawa *et al.*, 1996). SIMS data are given in Table 3.

RESULTS

As illustrated in Fig. 1 for Ti and Ce, the wall-rock section sampled for this study compares favourably with that

Table 1: Bulk-rock major- and trace-element analyses in the drilled wall-rock traverse

Sample:	EDL001	EDL002	EDL014	EDL041	EDL017	EDL019	EDL020	EDL024
Rock type:	dyke	dyke	dyke	dyke	am. harz.	am. harz.	am. harz.	am. harz.
Distance from the dyke–wall-rock boundary (cm):					3·1	9·3	12·1	15·5
wt %								
SiO_2	43·43	43·11	43·49	42·62	42·56	42·42	43·17	42·93
TiO_2	2·26	4·26	2·66	2·12	0·081	0·120	0·031	0·064
Al_2O_3	14·79	13·52	13·88	13·88	1·33	3·16	0·50	0·72
FeO	8·93	5·82	8·29	10·18	10·75	9·03	8·95	8·97
MgO	15·54	16·51	16·89	16·05	43·23	40·27	46·24	45·52
CaO	11·61	11·99	11·28	12·17	0·39	0·63	0·48	0·56
Na_2O	1·52	2·48	1·63	1·46	0·04	<0·01	<0·01	0·01
K_2O	0·36	0·98	0·48	0·32	<0·004	<0·004	<0·004	0·005
MnO	0·254	0·096	0·185	0·207	0·149	0·050	0·131	0·133
P_2O_5	0·036	0·042	0·033	0·036	0·020	0·012	0·014	0·014
LOI	1·72	1·58	1·36	2·54	0·55	1·41	1·96	2·29
Mg-no.	0·756	0·835	0·784	0·738	0·878	0·888	0·902	0·900
ppm								
Sc	54·5	41·7	40·4	44·7	4·2	5·6	4·1	5·0
V	266	313	298	321	26·8	98	17·6	22·5
Cr	390	360	500	489	1419	22587	1160	1618
Ni	345	612	469	392	2219	1973	2544	2558
Cu	94	31	80	99	3	4	1	13
Zn	28	27	45	85	62	133	44	51
Ga	14·0	14·2	15·7	17·6	3·1	5·8	0·7	1·6
Rb	1·30	2·04	1·53	1·12	0·17	0·13	0·05	0·25
Sr	208	452	298	234	4·4	5·0	3·6	4·5
Y	52	32	29	28	0·50	0·74	0·45	0·55
Zr	88	85	81	81	2·33	2·83	1·65	2·21
Nb	6·7	18·2	9·3	6·4	0·052	0·109	0·002	0·069
Ba	133	75	53	44	4	2	2	5
La	2·85	4·9		3·1	0·0061			
Ce	10·4	16·3	12·1	11·1	0·164	0·233	0·149	0·40
Nd	11·1	15·7	12·1	10·9	0·145	0·200	0·175	0·326
Sm	3·91	5·0	3·95	3·50	0·046	0·063	0·044	0·090
Eu	1·54	1·87	1·48	1·33	0·0172	0·0237	0·0162	0·0326
Gd	5·8	6·0		4·3	0·057			
Dy		5·8		5·1	0·075			
Er	6·2	3·13		2·85	0·059			
Yb	7·0	2·75	2·52	2·54	0·080	0·087	0·050	0·092
Lu	1·18	0·396		0·326	0·0140			
$^{87}Sr/^{86}Sr$		0·70269		0·70269	0·70291			0·70331
$^{143}Nd/^{144}Nd$	0·51304	0·51300		0·51301	0·51298		0·51292	0·51283
ε_{Sr} (100 Ma)		−24·27		−24·28	−23·13			−18·44
ε_{Nd} (100 Ma)	7·64	7·12		7·29	6·74		6·07	4·13

Sample:	EDL025	EDL028	EDL029	EDL030	EDL031	EDL032	EDL033	EDL034
Rock type:	am. harz.	(ap.) harz.	harzburgite	harzburgite	(ap.) harz.	harzburgite	harzburgite	harzburgite
Distance (cm):	16·9	29·5	31	34·9	38·7	43·2	45·8	45·8
wt %								
SiO_2	43·61	42·68	43·09	42·88	43·10	43·03	43·57	43·95
TiO_2	0·052	0·032	0·023	0·010	0·010	0·011	0·011	0·013
Al_2O_3	0·82	0·66	0·74	0·87	0·39	0·82	0·48	0·61
FeO	9·27	8·17	8·51	8·27	8·20	8·26	8·01	8·08
MgO	44·95	46·97	46·10	46·52	47·07	46·28	46·66	46·03
CaO	0·56	0·35	0·42	0·44	0·44	0·49	0·45	0·56
Na_2O	0·09	0·19	<0·01	<0·01	0·06	0·01	<0·01	<0·01
K_2O	<0·004	0·004	<0·004	<0·004	<0·004	<0·004	<0·004	<0·004
MnO	0·131	0·121	0·115	0·107	0·119	0·108	0·115	0·118
P_2O_5	0·015	0·017	0·024	0·023	0·028	0·028	0·039	0·038
LOI	1·56	2·46	2·30	1·92	2·00	1·47	1·39	1·58
Mg-no.	0·896	0·911	0·906	0·909	0·911	0·909	0·912	0·910
ppm								
Sc	5·5	4·8	5·2	5·6	5·4	6·6	6·1	7·0
V	26·1	20·9	24·6	34·0	17·9	39·6	22·3	26·8
Cr	2234	2077	2480	5554	1178	5579	1346	2078
Ni	2466	2647	2616	2601	2676	2627	2620	2566
Cu	6	<1	4	1	<1	8	2	1
Zn	54	53	52	63	46	62	45	49
Ga	1·6	1·3	0·5	2·5	0·8	1·4	0·9	1·0
Rb	0·13	<0·1	0·13	0·10	0·27	0·15	0·16	0·05
Sr	4·8	3·6	3·8	3·8	9·4	4·4	4·0	8·3
Y	0·57	0·41	0·20	0·21	0·24	0·06	0·15	0·19
Zr	2·21	1·31	0·58	0·35	0·30	0·35	0·34	0·36
Nb	<0·001	0·072	<0·001	<0·001	0·030	<0·001	<0·001	0·027
Ba	3	3	4	3	4	5	5	3
La	0·131	0·150					0·288	
Ce	0·37	0·39	0·51	0·64	0·65	0·95	0·86	0·95
Nd	0·279	0·207	0·304	0·39	0·39	0·59	0·54	0·61
Sm	0·071	0·041	0·054	0·062	0·060	0·093	0·090	0·105
Eu	0·025	0·0128	0·0161	0·0167	0·0157	0·0235	0·0225	0·0264
Gd	0·076	0·036						
Dy	0·087	0·045					0·038	
Er	0·056	0·036					0·0184	
Yb	0·070	0·051	0·050	0·0323	0·0217	0·0210	0·0213	0·0233
Lu	0·0118	0·0105					0·0039	
$^{87}Sr/^{86}Sr$		0·70397	0·70433	0·70475		0·70512		
$^{143}Nd/^{144}Nd$	0·51278	0·51252	0·51245	0·51234				0·512326
ε_{Sr} (100 Ma)			−2·72	3·71		8·51		
ε_{Nd} (100 Ma)	3·32	−1·32	−2·53	−4·53				−4·91

Table 1: continued

Sample:	EDL035	EDL036	EDL037	EDL038	EDL039	EDL040
Rock type:	ap. harz.	ap. harz.	ap. harz.	ap. harz.	ap. harz.	(ap.?) harz.
Distance (cm):	51·1	55·7	60·3	64·8	69·3	69
wt %						
SiO_2	43·57	43·48	43·26	43·56	43·14	46·13
TiO_2	0·016	0·022	0·018	0·022	0·041	0·063
Al_2O_3	0·59	0·52	0·47	0·64	0·80	1·34
FeO	8·38	0·52	0·47	0·64	0·80	1·34
MgO	46·09	46·62	46·54	46·35	46·21	42·81
CaO	0·50	0·46	0·45	0·47	0·37	0·82
Na_2O	<0·01	0·09	<0·01	0·02	0·03	0·02
K_2O	<0·004	<0·004	<0·004	<0·004	<0·004	<0·004
MnO	0·114	0·117	0·121	0·119	0·121	0·111
P_2O_5	0·043	0·047	0·049	0·053	0·057	0·042
LOI	1·35	1·06	0·92	1·42	1·36	0·91
Mg-no.	0·907	0·913	0·908	0·910	0·908	0·909
ppm						
Sc	6·7	6·3	6·2	6·3	4·6	9·7
V	28·2	22·8	21·4	26·2	27·5	49·7
Cr	2391	1418	1356	2092	2323	4330
Ni	2625	2596	2737	2599	2621	2740
Cu	1	1	20	1	2	208
Zn	50	46	46	50	53	53
Ga	0·9	0·6	1·8	1·0	1·6	2·3
Rb	0·18	0·12	0·17	0·05	0·11	0·22
Sr	5·3	4·7	4·7	4·6	4·0	7·7
Y	0·21	0·17	0·33	0·40	0·35	0·73
Zr	0·61	0·72	0·80	1·36	1·59	2·33
Nb	<0·001	<0·001	0·001	0·037	<0·001	0·053
Ba	2	4	4	6	4	3
La	0·346		0·375	0·45		0·68
Ce	1·04	1·04	1·02	1·18	1·08	1·98
Nd	0·63	0·61	0·58	0·66	0·58	1·14
Sm	0·110	0·107	0·102	0·121	0·105	0·202
Eu	0·0277	0·0271	0·0263	0·0325	0·0282	0·055
Gd	0·075		0·075	0·097		0·216
Dy	0·051		0·055	0·081		0·133
Er	0·0235		0·0254	0·041		0·063
Yb	0·0243	0·0247	0·0259	0·042	0·038	0·060
Lu	0·0039		0·0042	0·0065		0·0092
$^{87}Sr/^{86}Sr$	0·70519		0·70517			
$^{143}Nd/^{144}Nd$	0·512326		0·51233			0·5124
ε_{Sr} (100 Ma)	9·51		9·10			
ε_{Nd} (100 Ma)	−4·92		−4·86			−3·50

amp. harz., amphibole harzburgite; ap. harz., amphibole-free harzburgite with apatite positively identified by Woodland *et al.* (1996); (ap.) harz., amphibole-free harzburgite with apatite tentatively identified by Woodland *et al.* (1996); (ap.?) harz., sample EDL040 not studied by Woodland *et al.* (1996); harzburgite, amphibole- and apatite-free harzburgite. Mg-number = Mg/(Mg + Fe) cationic ratio. The analytical methods are given in the text.

Table 2: Bulk-rock trace-element analyses by ICP-MS in the wall-rock traverse studied by Bodinier et al. *(1990)*

Sample:	LH11-0	LH11-1	LH11-8	LH11-12	LH11-15	LH11-21	LH11-27	LH11-28	LH11-33	LH11-39	LH11-45	LH11-49	LH11-65
Rock type:	dyke	am. harz.	am. harz.	am. harz.	am. harz.	harzburgite	harzburgite	harzburgite	harzburgite	harzburgite	harzburgite	harzburgite	harzburgite
Distance (cm):	1	8	12	15	21	27	28	33	39	45	49	65	
ppm													
Rb	1·57	0·176	0·198	0·173	0·178	0·168	0·092	0·090	0·091	0·101	0·252	0·117	0·130
Sr	227	5·4	3·87	8·9	3·40	3·65	2·34	2·85	3·22	3·46	3·95	4·26	4·52
Y	16·0	0·75	0·476	0·96	0·321	0·207	0·085	0·081	0·063	0·099	0·152	0·147	0·392
Zr	53	3·44	2·26	5·5	1·46	0·88	0·311	0·237	0·226	0·261	0·51	0·55	1·71
Nb	9·9	0·082	0·076	0·101	0·0422	0·162	0·0335	0·0319	0·0365	0·0451	0·066	0·058	0·050
Cs	0·081	0·0100	0·0070	0·0061	0·0060	0·0080	0·0272	0·0028	0·0031	0·0037	0·0067	0·0049	0·0060
Ba	46·3	0·83	1·00	1·04	0·458	0·52	0·061	0·077	0·256	0·116	0·78	0·133	0·255
La	3·22	0·128	0·085	0·216	0·082	0·089	0·221	0·245	0·294	0·383	0·428	0·403	0·53
Ce	10·6	0·365	0·247	0·66	0·189	0·171	0·52	0·62	0·81	1·15	1·29	1·25	1·46
Pr	1·84	0·062	0·0403	0·111	0·0308	0·0218	0·055	0·068	0·092	0·155	0·178	0·174	0·194
Nd	10·1	0·342	0·208	0·57	0·154	0·098	0·165	0·203	0·300	0·56	0·66	0·69	0·81
Sm	2·99	0·109	0·070	0·177	0·0475	0·0320	0·0261	0·0278	0·0340	0·072	0·095	0·102	0·147
Eu	1·11	0·0405	0·0270	0·064	0·0183	0·0118	0·0073	0·0088	0·0102	0·0192	0·0240	0·0259	0·0413
Gd	3·56	0·138	0·086	0·213	0·059	0·0355	0·0199	0·0185	0·0173	0·0349	0·050	0·056	0·116
Tb	0·57	0·0236	0·0145	0·0329	0·0095	0·0061	0·0032	0·0030	0·0029	0·0051	0·0066	0·0070	0·0161
Dy	3·68	0·158	0·099	0·216	0·067	0·0415	0·0197	0·0171	0·0156	0·0230	0·0343	0·0351	0·090
Ho	0·72	0·0331	0·0213	0·0437	0·0143	0·0090	0·0044	0·0042	0·0031	0·0044	0·0062	0·0060	0·0173
Er	2·06	0·103	0·068	0·125	0·0471	0·0323	0·0154	0·0157	0·0113	0·0152	0·0226	0·0202	0·052
Tm	0·292	0·0165	0·0114	0·0189	0·0082	0·0059	0·0032	0·0031	0·0023	0·0026	0·0040	0·0033	0·0086
Yb	1·82	0·113	0·076	0·121	0·059	0·0450	0·0223	0·0208	0·0168	0·0166	0·0234	0·0221	0·052
Lu	0·292	0·0211	0·0148	0·0211	0·0113	0·0100	0·0054	0·0045	0·0042	0·0041	0·0053	0·0051	0·0093
Hf	1·81	0·129	0·070	0·178	0·0397	0·0324	0·0131	0·0121	0·0101	0·0099	0·0147	0·0207	0·0372
Ta	0·64	0·0083	0·0069	0·0117	0·0055	0·0105	0·0041	0·0039	0·0048	0·0063	0·0092	0·0085	0·0070
Pb	0·29	0·047	0·039	0·029	0·022	0·048	0·054	0·066	0·076	0·21	0·083	0·094	0·12
Th	0·123	0·0146	0·0109	0·0205	0·0098	0·0294	0·0135	0·0156	0·0168	0·0172	0·0214	0·0173	0·0366
U	0·0376	0·0053	0·0041	0·0056	0·0031	0·0058	0·0044	0·0040	0·0037	0·0039	0·0053	0·0038	0·0071

amp. harz., amphibole harzburgite; harzburgite, amphibole-free harzburgite (samples not searched for apatite by cathodoluminescence).

Table 3: In situ *analyses of trace elements by SIMS in cpx and amphibole of the drilled wall-rock traverse*

Sample:	EDL001					EDL016		EDL018		EDL022			
Rock type:	dyke					am. harz		am. harz.		am. harz			
						1·0		5·0		7·0			
Distance from the dyke–wall-rock boundary (cm):													
	CPX	CPX	CPX	AMPH.	AMPH.	CPX	CPX	CPX	CPX	CPX	CPX	CPX	AMPH.
ppm													
Ti	10180	8480	4650		29690	7660	10050	7690	8240	7420	9010	7660	25780
V	402	399	326		405	321	375	338	362	319	354	336	370
Cr	489	453	367		497	4110	4860	1810	6100	4680	6810	5040	4530
Sr	145	170	80		538	144	161	181	198	178	165	156	577
Y	15·1	13·2	28·3		17·1	19·2	25·2	19·2	24·6	19·9	21·8	20·4	27·6
Zr	164	147	125		77	128	149	174	208	122	152	137	78
La	2·89	2·36	2·43	8·2	9·1	3·93	4·62	5·4	4·52	3·97	3·56	3·98	8·2
Ce	9·9	7·9	8·5	28·4	30·6	12·3	14·8	15·6	13·7	10·8	10·8	12·5	25·0
Nd	9·0	6·7	7·5	28·4	31·9	9·6	11·8	12·7	11·0	6·9	7·0	8·3	21·2
Sm	3·42	2·49	2·97	8·6	9·7	3·31	4·49	4·02	3·59	2·24	2·67	2·76	6·2
Eu	1·34	0·95	1·13	4·23	4·40	1·30	1·63	1·49	1·36	0·90	1·06	1·08	1·08
Dy	2·86	1·88	2·79	6·1	6·4	3·52	4·46	4·14	3·30	2·12	2·80	2·99	5·8
Er	1·15	0·70	1·24	2·23	2·10	1·79	2·43	2·31	1·92	1·22	1·52	1·33	2·45
Yb	0·79	0·52	0·83	1·16	1·45	1·54	2·22	1·90	1·76	1·16	1·40	1·23	1·91

Sample:	EDL019		EDL024		EDL025			EDL027	EDL030	EDL031
Rock type:	am. harz.		am. harz.		am. harz.			am.-ap. h.	harzb.	(ap.) harz.
Distance (cm):	9·3		15·5		16·9			23·0	34·9	38·7
	CPX	CPX	CPX	CPX	CPX	CPX-c	CPX-r	AMP.	CPX	CPX
ppm										
Ti	3190	1890	4290	5360	3510	2480		24260	296	310
V	381	280	361	347	368	292		494	328	371
Cr	12920	9780	6880	9000	11060	12740		8900	15350	10830
Sr	202	134	128	168	172	259		485	199	172
Y	16·9	13·8	15·8	17·2	16·4	13·3		22·2	7·3	6·4
Zr	98	74	117	115	100	78		80	14·5	12·0
La	2·66	3·62	4·92	6·1	3·82	7·6	3·48	24·1	9·9	17·7
Ce	7·4	10·3	17·1	18·3	11·6	21·1	9·2	65·4	29·9	55·6
Nd	6·3	7·3	11·4	11·9	7·5	13·1	5·7	38·7	16·8	29·6
Sm	2·10	2·53	3·51	3·59	2·42	3·87	1·88	8·7	3·10	5·4
Eu	0·83	0·90	1·39	1·42	0·73	1·23	0·60	1·03	0·79	1·58
Dy	2·87	2·53	3·15	3·08	1·73	2·30	1·53	7·6	0·93	2·11
Er	1·43	1·36	1·98	1·75	0·73	1·23	0·58	3·01	0·72	1·64
Yb	1·42	1·28	1·63	1·49	0·95	1·17	0·72	2·80	0·431	1·08

Sample:	EDL033				EDL037		EDL039	
Rock type:	harzb.				ap. harz.		ap. harz.	
Distance (cm):	45·8				60·3		69·3	
	CPX	CPX-c	CPX-r	CPX-r	CPX	CPX	CPX	CPX
ppm								
Ti	403	286	287		1020	980	4470	5710
V	426	318	322		347	336	419	499
Cr	9110	14230	14020		13960	13540	12670	11090
Sr	143	197	229		164	197	212	169
Y	8·0	6·5	6·7		11·0	11·1	15·3	17·1
Zr	20·3	14·3	14·7		56	58	121	158
La	11·6	19·3	17·1	16·0	12·3	15·7	12·4	9·8
Ce	38·1	62·0	56·0	47·9	43·2	54·2	38·2	29·4
Nd	22·1	38·4	32·1	26·5	25·6	32·2	21·7	16·1
Sm	4·79	6·3	6·1	5·5	5·3	7·1	5·6	3·81
Eu	1·39	1·57	1·56	1·37	1·51	2·11	1·56	1·16
Dy	2·18	1·69	2·05	1·98	2·81	3·43	3·00	2·15
Er	1·27	1·54	1·48	1·26	1·77	2·18	1·33	1·04
Yb	0·72	0·76	0·87	0·81	1·06	1·35	1·21	0·94

amp. harz., amphibole harzburgite; amp.-ap. h., apatite-bearing amphibole harzburgite; ap. harz., amphibole-free harzburgite with apatite positively identified by Woodland *et al.* (1996); (ap.) harz., amphibole-free harzburgite with apatite tentatively identified by Woodland *et al.* (1996); harzb., amphibole- and apatite-free harzburgite. CPX and AMPH., core analyses of individual clinopyroxene and amphibole grains; CPX-c and CPX-r, core and rim analyses in single clinopyroxene grains.

studied by Bodinier *et al.* (1990) with regard to major-, minor- and trace-element variations in bulk rocks. This indicates that the metasomatic zones defined by Bodinier *et al.* show some continuity along the dyke, at least over the distance (~60 cm) between the two sections. At less than ~20–25 cm from the dyke–wall-rock boundary, the amphibole peridotite displays decreasing concentrations of Fe, Ti, Mn, Al, Ca, Na and HREE, and increasing concentrations of Mg and Ni away from the dyke (Table 1). Further in the wall-rock, these elements show nearly constant concentrations in the amphibole-free harzburgite. The Al, Ca, Na and HREE contents are low, consistent with the refractory character of the wall-rock (e.g. Al_2O_3 mostly $<1\%$ and HREE $<0{\cdot}1\times$ chondritic abundances). In contrast to the moderately incompatible elements, such as Ti and HREE, more incompatible elements, such as LREE and P, show increasing abundances from the dyke border throughout the wall-rock (0–70 cm, Fig. 1). The highest phosphorus content ($>0{\cdot}045\%$ P_2O_5 at >50 cm from the dyke) is found in samples in which apatite was positively identified by Woodland *et al.* (1996).

The ICP-MS data for the section previously studied by Bodinier *et al.* (1990) confirm the strong variability of trace elements that had been already demonstrated for REE (Table 2 and Fig. 2). The amphibole harzburgite shows flat, or slightly convex-upward, primitive mantle-normalized trace-element patterns. The trace-element patterns in the wall-rock mimic that of the dyke at lower concentration, except for higher Th and U relative to LREE and the lack of a positive Nb–Ta anomaly. The La_N/Yb_N ratio is in the range 0·8–1·3 for the amphibole harzburgite (<20 cm). Further in the wall-rock, the amphibole-free harzburgite is characterized by a strong enrichment in LREE relative to HREE ($La_N/Yb_N = 7{\cdot}1$–$16{\cdot}6$). Th and U are enriched in comparison with the amphibole harzburgite, although at a lesser degree than the LREE. Similarly, Sr tends to be less enriched than the LREE whereas Ba is strongly depleted in the amphibole-free harzburgite zone. The high field strength elements (HFSE: Nb, Ta, Zr and Hf in Fig. 2) show negative anomalies relative to REE and Th–U. LREE-enriched, HFSE-depleted trace-element patterns have been frequently reported from mantle xenoliths, where they are generally ascribed to carbonate metasomatism (Dautria *et al.*, 1992; Hauri *et al.*, 1993; Ionov *et al.*, 1993; Rudnick *et al.*, 1993). The resemblance to carbonate-melt metasomatism is enhanced by the presence of apatite (Woodland *et al.*, 1996).

Two representative harzburgites from Lherz were also analysed by ICP-MS at Montpellier. As far as we can tell, these samples are spatially unrelated to dykes and veins.

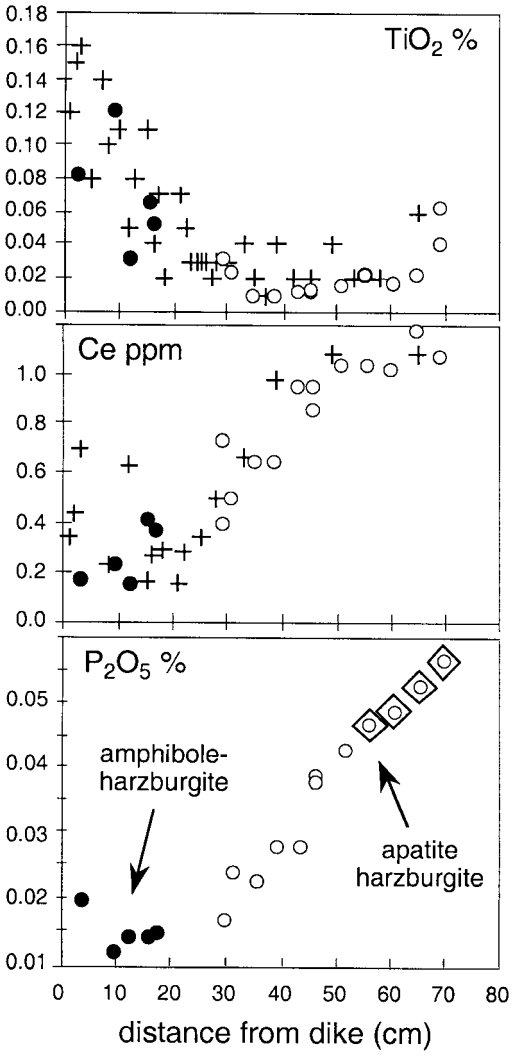

Fig. 1. Variations of TiO_2, Ce and P_2O_5 vs distance from the dyke–wall-rock boundary. The samples drilled for this study are shown by circles: •, amphibole harzburgite; ○, amphibole-free harzburgite. The samples in which apatite was positively identified by Woodland *et al.* (1996) are distinguished by diamonds on the P_2O_5 diagram. On the TiO_2 and Ce diagrams are also shown the variations reported by Bodinier *et al.* (1990) for a different traverse of the same wall-rock, for comparison (+).

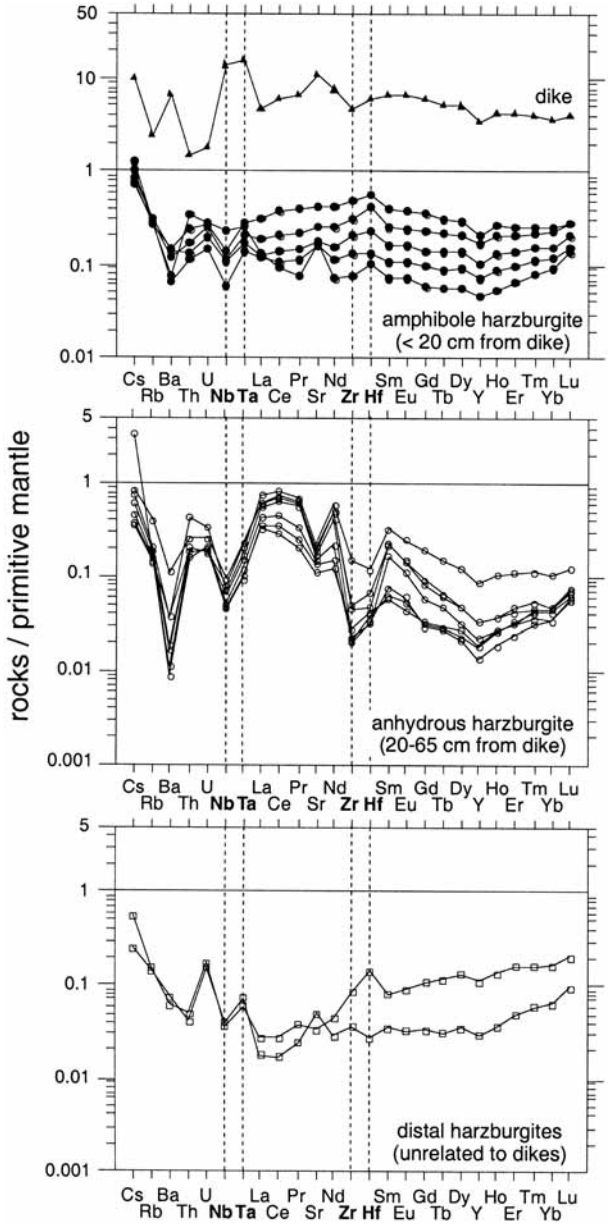

Fig. 2. Primitive mantle-normalized, trace-element composition of the wall-rock samples previously studied by Bodinier *et al.* (1990) and re-analysed by ICP-MS during this study. Two distal harzburgites [samples 71-125 and 73-104 of Bodinier *et al.* (1988)] were also re-analysed for comparison. As far as we can tell, these samples are spatially urelated to dykes. Normalizing values after Sun & McDonough (1989).

Like many mantle harzburgites worldwide (e.g. Bodinier & Godard, ~~2004~~), they display U-shaped normalized trace-element patterns. In contrast with the wall-rock harzburgite, they are depleted in the LREE and lack negative HFSE anomalies (Fig. 2).

In agreement with the bulk-rock trace-element data, the ion microprobe analyses (Table 3 and Fig. 3) show a progressive increase in the LREE/HREE ratio in cpx away from the dyke, with a maximum La_N/Yb_N ratio in the range 14–18 at 30–60 cm distance. This variation is merely a reflection of a significant increase in the concentration of the LREE in cpx. Chondrite-normalized La, Ce and Nd contents increase from 10–30 × chondrite proximal to the dyke (i.e. <20 cm), to 40–110 × chondrite distal to the dyke (i.e. >30 cm). Conversely, Zr and Ti in cpx (and to a lesser degree HREE) decrease markedly and reach a minimum $Zr_N = 3$–5 distal to the dyke (30–60 cm) compared with 20–50 proximal to the dyke (<20 cm). These variations result in

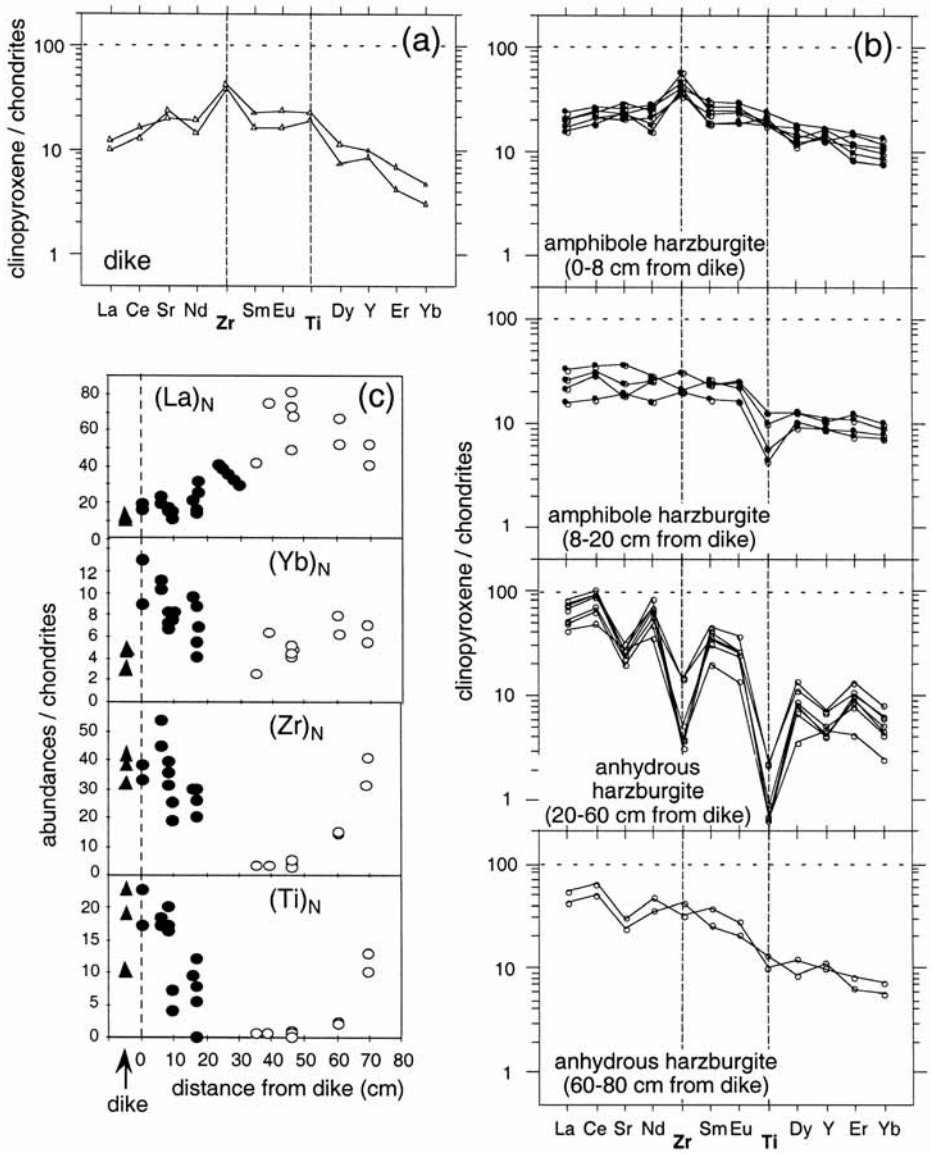

Fig. 3. Ion-microprobe trace-element analyses of clinopyroxene in the samples drilled for this study. (a) and (b) Chondrite-normalized trace-element patterns of cpx in dyke and wall-rock; (c) variation of normalized La, Yb, Zr and Ti abundances in dyke and wall-rock cpx vs distance from dyke. Normalizing values after Sun & McDonough (1989).

markedly different chondrite-normalized trace-element patterns for cpx. In the amphibole peridotite (< 20 cm from the dyke) the cpx patterns are mildly fractionated, slightly convex and smooth in shape, except for a subtle positive anomaly of Zr (Zr_N/Sm_N = 1·3–2·3). In contrast, cpx from the amphibole-free peridotite (> 30 cm) has strongly fractionated (LREE-enriched) trace-element patterns with negative Zr and Ti anomalies. At 30–60 cm from the dyke, the Zr_N/Sm_N and Ti_N/Dy_N ratios in cpx are systematically lower than 0·1. On the other hand, these anomalies at not present at > 60 cm, where the HREE tend to increase. In the most distal samples (60–80 cm), the trace-element patterns of cpx show a steady increase from HREE to LREE without significant HFSE anomalies. The strong LREE enrichment of cpx in the anhydrous harzburgite rules out chemical equilibrium with the parental melt of the dyke. Coupled with the negative Zr and Ti anomalies, this enrichment suggests equilibrium with carbonate melt.

With the exception of Zr, the trace-element composition of the amphiboles (Table 3) mimics that of cpx from the same samples, but the concentrations are generally higher ($K^{amph/cpx}$ = 0·8–1·5 for Y, V and Cr, 1·5–2·5 for HREE, 2–4 for LREE, and 3–4 for Sr and Ti). Zr is depleted in amphibole relative to cpx ($K^{amph/cpx}$ = 0·5–0·6). These values are consistent with the

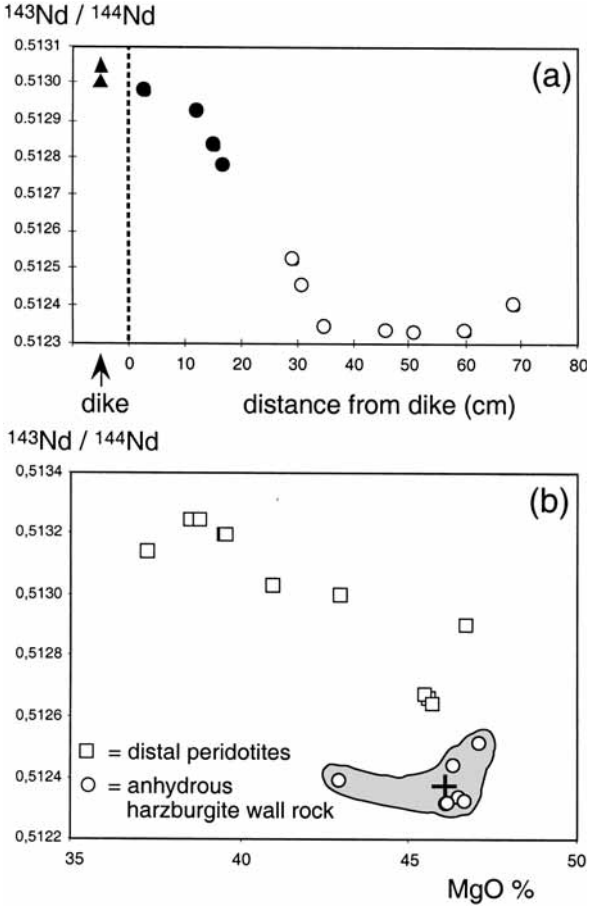

Fig. 4. (a) Variation of $^{143}Nd/^{144}Nd$ in the dyke and wall-rock samples drilled for this study vs distance from dyke. Symbols as in Fig. 2. (b) Plot of $^{143}Nd/^{144}Nd$ vs MgO (on a 100% anhydrous basis) for the apatite harzburgite samples (>25 cm from dyke) and distal peridotites from Lherz and neighbouring peridotite bodies (Bodinier *et al.*, 1988; Downes *et al.*, 1991; McPherson *et al.*, 1996). As far as we can tell, the 'distal' peridotites are spatially urelated to dykes. The Nd isotopic value reported by Downes *et al.* (1991) for the 20–65 cm, amphibole-free harzburgite wall-rock [measured on cpx separates from the traverse studied by Bodinier *et al.* (1990)] is also shown for comparison (+).

amphibole/cpx relationships observed in other mantle rocks and experimental runs (e.g. Witt-Eickschen & Harte, 1994; Ionov & Hofmann, 1995; Tiepolo *et al.*, 2001), indicating that inter-mineral chemical equilibrium was achieved in the amphibole harzburgite wall-rock.

The contrasted geochemical signatures of the spatially juxtaposed amphibole and apatite peridotites are also emphasized by their Nd–Sr isotope compositions (Table 1 and Fig. 4a). Proximal to the dyke–wall-rock contact (<10 cm), the wall-rock has an isotopic signature ($\varepsilon_{Nd} = 6–7$; $\varepsilon_{Sr} = -20$ to -25) comparable with that of the dyke itself and other amphibole pyroxenites in Lherz (Downes *et al.*, 1991; Mukasa *et al.*, 1991; McPherson *et al.*, 1996). Distal to the dyke, the isotopic composition evolves towards more enriched values, reaching $\varepsilon_{Nd} = -5$ and $\varepsilon_{Sr} = +10$ at >20 cm. The low $^{143}Nd/^{144}Nd$ of the anhydrous harzburgite requires time-integration of low Sm/Nd ratios (i.e. LREE enrichment) over periods of ~900–1100 Myr (DMM model age and dyke–wall-rock 'isochron' age, respectively) and, as such, cannot have formed in the time frame of dyke emplacement in the Cretaceous (100 Myr; Goldberg *et al.*, 1986). Insufficient time has elapsed since the formation of the dyke to generate the isotopic variability by time-integration of the LREE enrichment. On the other hand, in Lherz and other orogenic lherzolites, the peridotites unrelated to dykes and pyroxenite layers show a negative correlation between Nd–Sr isotopic enrichment and 'fertility' (Fig. 4b; Downes *et al.*, 1991; Reisberg & Lorand, 1995; Bodinier & Godard, 2004). The enriched isotopic signature of the distal anhydrous peridotite is consistent with the refractory, harzburgitic composition of the wall-rock and is therefore considered to represent the isotopic signature of the wall-rock protolith before dyke emplacement. The correlation of the $^{143}Nd/^{144}Nd$ ratio vs MgO suggests that the isotopic enrichment of the harzburgite protolith is somehow linked to the formation of the tabular harzburgites. Conversely, the proximal samples collected at <20 cm from the dyke plot away from the correlation and were clearly contaminated during dyke emplacement.

DISCUSSION

Trace-element variations somewhat comparable with those observed in the Lherz wall-rock have been reported from several suites of mantle xenoliths, in several instances amphibole- and apatite-bearing peridotites (e.g. Hauri *et al.*, 1993; Bedini *et al.*, 1997; Zangana *et al.*, 1997; Baker *et al.*, 1998; Xu *et al.*, 1998; Ionov *et al.*, 2002*a*). Bedini *et al.* (1997) observed similar variations in xenoliths from the East African Rift, which correlate with textural/mineralogical features and equilibrium temperatures. In mantle xenoliths, flat trace-element patterns (i.e. abundance normalized to primitive mantle) are generally observed in relatively high-T, apatite-free samples whereas the large ion lithophile element (LILE)-enriched, HFSE-depleted signature is typical of lower-T, apatite-bearing samples. Bedini *et al.* (1997) ascribed this variation to a kilometre-scale, single-stage process involving gradual solidification of melt infiltrated into the lithospheric mantle through successive melt–rock reactions down a conductive, thermal gradient. This process would be associated with strong chemical evolution of the melt, from an originally basaltic composition to progressively volatile-enriched compositions, culminating in low-T, small-volume carbonate melts. Harte *et al.* (1993) suggested that most metasomatic agents in mantle rocks may be formed by vein crystallization and 'percolative fractional crystallization' of ocean island basalt (OIB)-type primary

melts. Similarly, Baker *et al.* (1998) attributed the amphibole–apatite-bearing peridotites at Ataq, Yemen, to interaction between lithosphere and small-volume melts derived from the Afar plume partial melts.

The reactive porous flow model is supported by trace-element modelling (Bedini *et al.*, 1997; Vernières *et al.*, 1997). However, the ultra-enriched LREE and Th–U compositions (e.g. $\geq$100 $\times$ chondrite values for LREE in cpx) are well above the content expected for equilibrium with basaltic melt. This can be explained by the coupled effects of melt movement and reactions at decreasing melt mass, as also suggested by Harte *et al.* (1993). In contrast, HREE and compatible elements would be buffered by the peridotite minerals (olivine, opx, cpx), and the HFSE and Rb–Ba by very small amounts of Ti-oxides or amphibole, and phlogopite, respectively. Ionov *et al.* (2002*a*) used a similar approach to explain the coexistence of mildly LREE-enriched, amphibole-bearing peridotites and strongly LREE-enriched peridotites containing only sparse amphibole in a suite of mantle xenoliths from Spitsbergen. Such modelling can be applied to the Lherz wall-rock to account for the observed trace-element variation with a single-stage process. However, in Lherz the distance of percolation would be shorter than that envisioned in previous models, especially by Bedini *et al.* (1997). On the other hand, because the host peridotites were at a temperature of about 900–1000°C during dyke emplacement (Vétil *et al.*, 1988; Fabriès *et al.*, 1991), the wall-rock probably experienced a similar temperature gradient to that envisioned by Bedini *et al.* (i.e. a few hundred degrees).

The aim of modelling applied to the Lherz wall-rock is to reproduce the ultra-enrichment of LREE within the distal apatite-bearing peridotite while keeping the isotopic contamination from the dyke restricted to the proximal amphibole peridotite. The model assumes distinct origins and timing for chemical (LREE) and isotopic (Sr–Nd) enrichments in the anhydrous harzburgite. The LREE enrichment is considered to be related to dyke emplacement in the Cretaceous whereas the isotopic enrichment (low $^{143}Nd/^{144}Nd$–high $^{87}Sr/^{86}Sr$) is a signature of the wall-rock protolith. We shall thereafter discuss alternatives to this model, which consider that LREE enrichment occurred before dyke injection in the wall-rock protolith, being linked with isotopic enrichment.

THEORETICAL MODELLING

Previous studies used porous-flow models to explain trace-element variations in mantle xenoliths similar to those observed in the Lherz wall-rock (e.g. Bedini *et al.*, 1997; Ionov *et al.*, 2002*a*). In the present study, we focused on reproducing bulk-rock and cpx Nd abundances and $^{143}Nd/^{144}Nd$ variations in the wall-rock. The following terms will be used to describe the various aspects of dyke–wall-rock reaction.

Wall-rock protolith. Pre-existent harzburgite with a Nd content and $^{143}Nd/^{144}Nd$ ratio equivalent to the harzburgites spatially unrelated to dykes and veins in Lherz.

Dyke. Garnet–clinopyroxene assemblage formed by crystallization of a basaltic melt at high P and T.

Infiltrated zone. Wall-rock infiltrated by melt from the main dyke or volatile-rich derivatives where the protolith composition was modified by diffusional re-equilibration with infiltrated melt and/or percolation-reaction mechanisms.

Amphibole harzburgite reaction zone. Zone of modified wall-rock proximal ($<$20 cm) to the main dyke, where amphibole ($\pm$cpx) is precipitated in sheared peridotite. The Nd content and $^{143}Nd/^{144}Nd$ ratio are mainly controlled by variable degrees of re-equilibration with infiltrated melt.

Apatite harzburgite reaction zone. Zone of modified wall-rock distal ($>$20 cm) to the main dyke, where apatite is precipitated in less sheared peridotite. In this zone, Nd abundance and $^{143}Nd/^{144}Nd$ ratio are governed by the coupled effects of melt transport and amphibole precipitation. Consequently, the abundance of Nd is relatively high, but the $^{143}Nd/^{144}Nd$ ratio remains close to the protolith value.

Background and assumptions

The variation of $^{143}Nd/^{144}Nd$ in the Lherz wall-rock (Fig. 4a) can be simulated with a one-dimensional (1D) chromatographic model developed by Vasseur *et al.* (1991), which has been recently applied to isotope systems (Ionov *et al.*, 2002*b*). The main assumptions in this model are explained elsewhere (Bodinier *et al.*, 1990); some additional assumptions for the modelling of isotopes include the following.

Composition of the peridotite protolith. The Nd content of the pre-existent wall-rock protolith was fixed from the composition of harzburgites unrelated to dykes and veins in Lherz (Fig. 2). Based on the $^{143}Nd/^{144}Nd$ vs MgO correlation in Lherz peridotites (Fig. 4b), the $^{143}Nd/^{144}Nd$ ratio of the protolith is assumed to be that of the wall-rock at 30–50 cm from the dyke.

Composition of the infiltrated melt. The melt infiltrated in the wall-rock was probably evolved as a result of the precipitation of anhydrous minerals (pyroxene and garnet) in the dyke. This early derivative was very probably similar to the parental melt of the lherzites, suggesting that it was enriched in volatiles (water) and LILE compared with the parental melt of the dyke. However, the lherzites are virtually indistinguishable from the amphibole from the dykes in term of REE (Bodinier *et al.*, 1987*a*). Moreover, REE partitioning between amphibole and cpx in the dyke is consistent with published values

(Witt-Eickschen & Harte, 1994; Ionov & Hofmann, 1995; Tiepolo *et al.*, 2001). This suggests that melt evolution as a result of mineral segregation in the dyke was associated with only minor LREE enrichment. Alternatively, the anhydrous minerals were re-equilibrated with the parental melt of the lherzites owing to pervasive percolation of the water-rich derivative in the dyke itself. This second alternative was suggested by Harte *et al.* (1993) for composite mantle xenoliths. It is supported by textural evidence for the replacive (metasomatic) character of the amphibole in the dyke. In both hypotheses, the composition of cpx in dyke can be used to establish the Nd content of the infiltrated melt. Its $^{143}Nd/^{144}Nd$ ratio is assumed to be that of the dyke.

Partition coefficients. The mineral/melt partition coefficients (K_d) of Nd are considered to be constant (although the 'plate model', for instance, allows variation of this parameter). The chemical evolution of melt in the wall-rock towards water-rich and/or carbonatitic compositions probably resulted in variations of the K_d values for trace elements. However, the variations are expected to be moderate for REE compared with other trace elements such as LILE and HFSE. Moreover, the exact composition of melt derivatives in the wall-rock is poorly constrained. Therefore, our approach was to try to reproduce the Nd variations with a simple model, assuming constant K_d values, and to modify the K_d values only if the simple approach proved to be unsuccessful.

Age corrections. Age corrections are moderate ($\leq$10%) because of the relatively young age of dyke injection and emplacement of the massif ($\sim$100 Ma). Uncorrected $^{143}Nd/^{144}Nd$ ratios were used for modelling.

All simulations indicate the existence of a chromatographic Nd isotopic front at some distance behind a melt infiltration front (Fig. 5). Behind the Nd isotopic front, the isotopic composition of the harzburgite protolith has re-equilibrated with the infiltrated melt. In contrast, ahead of the front, the percolating melt has re-equilibrated with the harzburgite protolith. Nevertheless, it should be noted that the chromatographic front does not constitute a sharp boundary between these two domains. Rather it is a transition zone, $\sim$5–10 cm wide. The width of the chromatographic front is governed by element diffusivity in peridotitic minerals and interstitial melt. Wider fronts result either from slow diffusivity in minerals and/or efficient diffusivity in interstitial melt (Bodinier *et al.*, 1990; Vasseur *et al.*, 1991). Consistent with chromatographic theory (Navon & Stolper, 1987), our results indicate that the distance of the Nd chromatographic front behind the melt infiltration front depends on two main parameters: (1) bulk peridotite/melt Nd partition coefficient (D) and (2) melt fraction. Figure 5 illustrates the effect of these parameters. For a refractory mineralogy (i.e. 1% cpx, 0% amphibole; low D value) and a relatively high melt fraction (1%), the Nd front is close to the percolation front. To account for the existence of a chromatographic front at $\sim$20 cm from the dyke–wall-rock contact, the distance of melt percolation should not exceed $>$25 cm away from the contact. However, the presence of a few per cent amphibole, as is observed in the wall-rock, and/or melt fraction values significantly smaller than 1% result in a considerable change in the location of the Nd front relative to the melt front. A 'best fit' of the $^{143}Nd/^{144}Nd$ ratios with this model is shown in Fig. 6a. This was obtained with the following set of parameters: distance of the melt front from the melt source (dyke) ~~m,~~ melt fraction 0·1% and amphibole fraction 4%.

Non-reactive models (i.e. no melt–rock reaction)

The application of the 1D chromatographic model to the $^{143}Nd/^{144}Nd$ isotopic variations in the Lherz section has several drawbacks. First of all, the modelled chromatographic front is steeper than the $^{143}Nd/^{144}Nd$ variation observed in the wall-rock (Fig. 6a). A 'smoother' pattern could be obtained by decreasing the Nd diffusion coefficient in the minerals, but this would require chemical disequilibrium between melt and minerals whereas SIMS data indicate near-equilibrium, as attested by almost identical Nd content in cpx in the dyke and in the amphibole harzburgite (Table 3 and Fig. 3). Alternatively, to explain smoother patterns one could invoke efficient 'interstitial diffusive dispersion' of the elements (Bodinier *et al.*, 1990, and references therein), but we lack the experimental data to constrain the actual value of this parameter. However, the main weakness in this application is apparent in Fig. 6b, where we compare the measured Nd abundance in cpx with the model predictions based on the best-fit parameters in Fig. 6a. It is clear from this diagram that the 'best fit' obtained for the isotopes does not fit with the Nd concentrations. The calculated Nd abundances in cpx are much lower than those measured by SIMS, which implies that the minerals are far from being in chemical equilibrium with the melt. This result is a reflection of the slow diffusivity of Nd in minerals and of the relatively low melt/rock ratios in the model (i.e. 1% at 10 cm). As illustrated in Fig. 6b (dashed lines), the Nd concentration in cpx can be modified as follows.

(1) *Duration of the infiltration process*. This was increased by a factor of ten (i.e. 1000 years), which requires a decrease in the interstitial melt velocity from 1 to 0·1 cm/year if the distance of percolation is kept constant at 1 m. However, in this case only the cpx adjacent to the dyke ($<$1 cm) is re-equilibrated (Fig. 6b). Further from the dyke, the Nd concentration in cpx decreases and reaches the lowest value of the 'best-fit' model at about 10 cm. Moreover, increasing the duration of the infiltration

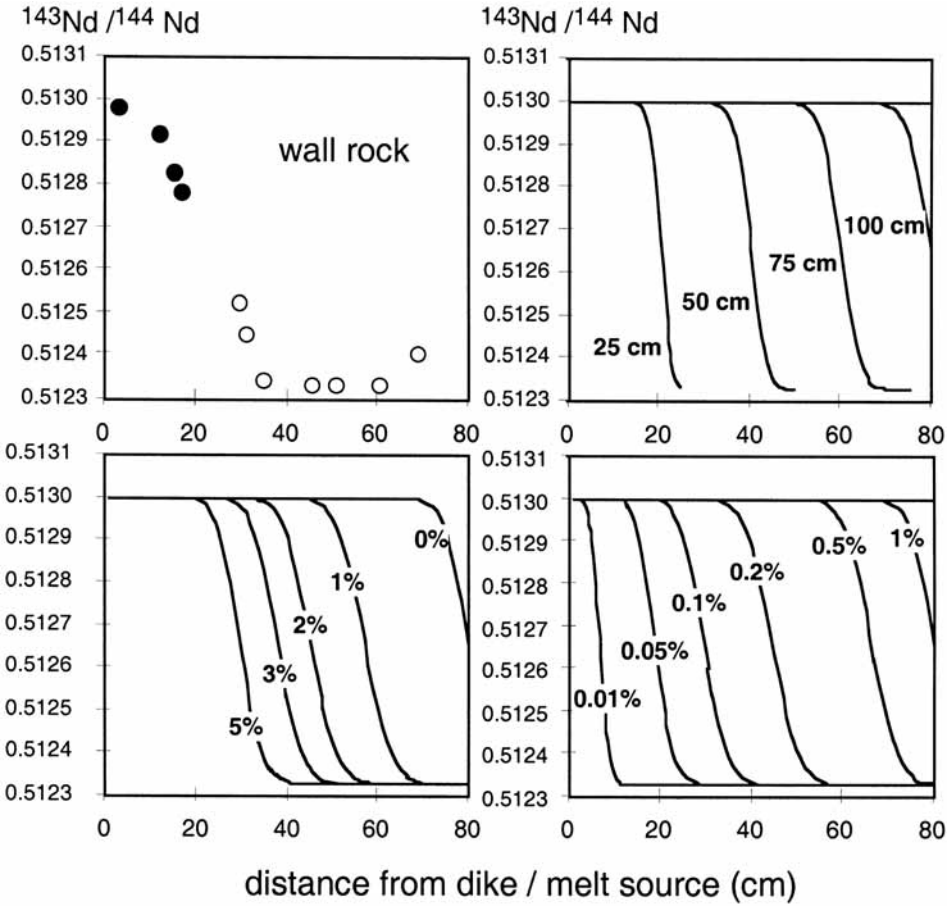

Fig. 5. Application of the 1D chromatographic model (Navon & Stolper, 1987) to the Nd isotopic variation in the wall-rock (top left diagram), using the numerical approach outlined by Bodinier *et al.* (1990) and Vasseur *et al.* (1991). The method simulates melt percolation in the intergranular space of a porous matrix at a given rate until the first batch of melt arrives at a fixed distance. The model assumes mineral–melt chemical equilibration at the surface of mineral grains (considered to be spherical) and element transport in minerals by diffusion. Trace-element concentrations in the interstitial melt are considered to be homogeneous on the scale of 'Representative Elementary Volumes' (REV; de Marsily, 1986), because diffusion in the melt is several orders of magnitude more rapid than in the minerals. Similarly, isotopic ratios in melt and minerals are assumed to homogenize instantaneously within individual REVs. The diffusion coefficients in solid and melt ($D_S = 10^{-13}$ cm^2/s and $D_L = 2 \times 10^{-8}$ cm^2/s, respectively) and the mineral radii ($a_{olivine} = a_{opx} = 0{\cdot}075$ cm; $a_{cpx} = 0{\cdot}0125$ cm) are identical to the values used by Bodinier *et al.* (1990). The mineral/melt partition coefficients of Nd are 0·00007 for olivine, 0·009 for opx, 0·1873 for cpx and 0·6 for amphibole. The olivine and opx values are from Kelemen *et al.* (1993), the cpx values from Hart & Dunn (1993). The amphibole values were obtained by combining the cpx/melt values from Hart & Dunn (1993) with inter-mineral amphibole/cpx values estimated from our SIMS data (Table 3). The modal composition of the wall-rock protolith is olivine 0·79, orthopyroxene 0·20, clinopyroxene 0·01. Based on the assumptions explained in the text, the Nd content and the $^{143}Nd/^{144}Nd$ ratio of the infiltrated melt were fixed at 48 × chondrite and 0·513, respectively, and the Nd content and $^{143}Nd/^{144}Nd$ ratio of the wall-rock protolith at 0·05 × chondrite and 0·51233. The results shown in the top right diagram were calculated with a melt fraction (= porosity) of 1%, a melt velocity of 1 cm/year and variable distance of melt infiltration, from 25 to 100 cm (hence different durations of the infiltration process, from 25 to 100 years). The results shown in the bottom left diagram were calculated with the same porosity and melt velocity values, for a distance of melt infiltration of 100 cm, but consider the presence of variable amount of amphibole in the wall-rock (0–5%). The models in the bottom right diagram were calculated with the same set of parameters (except for the lack of amphibole) and show the effect of variable porosity values, from very small melt fractions (0·01%) to relatively large fractions (1%).

process results in a $^{143}Nd/^{144}Nd$ front that is too close to the dyke, when compared with the data for Lherz (Fig. 6a). A reduction in amphibole proportion is required to balance this effect (Fig. 5).

(2) *Melt/rock ratio*. Increasing the melt/rock ratio can be achieved by increasing the melt fraction to 1%, or the distance of percolation to 2 m. In both cases (Fig. 6b), the model accounts for the abundance of Nd in the amphibole peridotite (< 25 cm from the dyke). However, the $^{143}Nd/^{144}Nd$ fronts are displaced to a greater distance from the dyke (Fig. 6a).

Most importantly, none of these models reproduces the strong enrichment in Nd observed in the distal amphibole-free peridotite at > 30 cm. This result is not

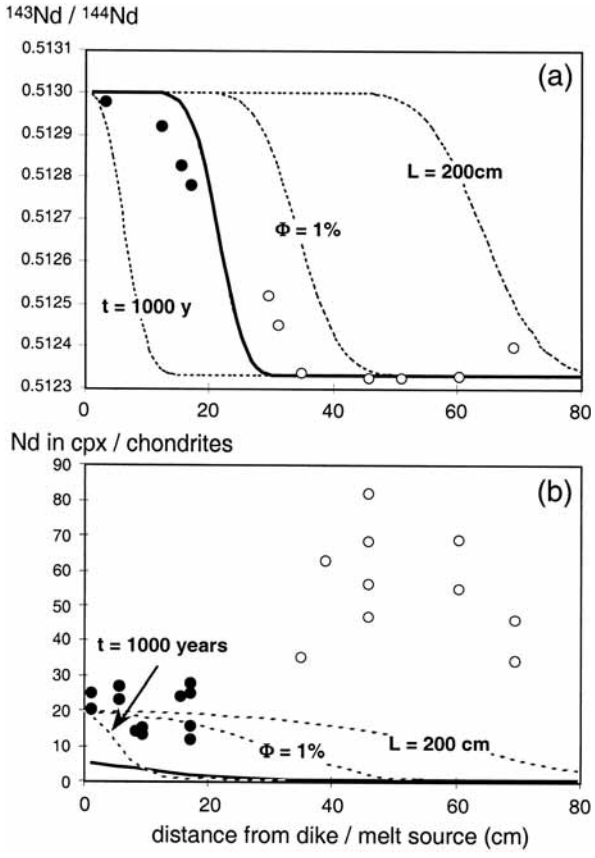

Fig. 6. (a) Best fit of the Nd isotopic variation in the wall-rock with the 1D chromatographic approach (bold continuous line). The observed $^{143}Nd/^{144}Nd$ variation is best explained with the following combination of parameters: L (distance of melt infiltration) = 100 cm, t (duration of melt infiltration) = 100 years, Φ (porosity, = melt fraction) = 0·1%, modal composition involving 4% amphibole. The other parameter values are given in Fig. 5 caption. The dashed lines show the effects of modifying some parameter values to improve the fit of Nd concentrations in clinopyroxene [shown in (b)]. (b) Bold continuous line shows Nd content in clinopyroxene calculated with the 1D chromatographic model and the set of parameters selected to fit the $^{143}Nd/^{144}Nd$ variation [shown in (a)]. The ion microprobe data obtained for clinopyroxene are shown for comparison. Dashed lines show results obtained by modifying some parameter values to increase the Nd content in clinopyroxene while trying to keep the $^{143}Nd/^{144}Nd$ variation consistent with the measured values [shown in (a)].

surprising, as the non-reactive model cannot account for trace-element abundances higher than those in equilibrium with the infiltrated melt (i.e. 'ultra-enriched' compositions).

Reactive models (with melt–rock reaction)

Strongly enriched trace-element abundances can be produced by melt infiltration mechanisms that involve melt–rock reactions at decreasing melt mass (Bedini *et al.*, 1997; Ionov *et al.*, 2002*a*). This results in gradual solidification of the melt in the infiltrated peridotite, a process also known as 'percolative fractional crystallization' (Harte *et al.*, 1993). In the Lherz wall-rock, evidence for this process is provided by the presence of secondary amphibole and cpx in the amphibole harzburgite zone (< 25 cm from the dyke; Bodinier *et al.*, 1990; Woodland *et al.*, 1996). Godard *et al.* (1995) predicted that the combination of melt transport and reaction would result in strong enrichments of incompatible elements that would be spatially disconnected from the reaction domain. For the most incompatible elements (i.e. for chromatographic fronts moving faster than the reaction front), the enrichment is expected to occur between the chromatographic front and the reaction front (Godard *et al.*, 1995, fig. 1a and b). In this scenario, the enrichment in highly incompatible elements in the Lherz wall-rock would occur beyond the amphibole peridotite and may account for the enrichment in the amphibole-free peridotite.

To evaluate this hypothesis, we investigated the effect of amphibole precipitation on the variations in the abundance of Nd and $^{143}Nd/^{144}Nd$ isotope ratio in the wall-rock using the 'plate model' of Vernières *et al.* (1997). In this model, melt transport is not considered as a function of time and distance but simulated by propagation of melt batches through macrovolumes of mantle rock. The plate model cannot be used to provide space and/or time constraints for the considered process. On the other hand, this approach allows the simulation of complex melt–rock reaction processes (e.g. Bedini *et al.*, 1997; Xu *et al.*, 1998).

To illustrate the effect of reaction (i.e. amphibole precipitation), the model was initially run without reaction. This first step is useful because it helps establish the number of cells for the model. Because the model assumes homogeneous mineral and melt compositions within individual reaction cells after each increment of melt transport and reaction, the number of cells in a given percolation column is a reflection of the efficiency of melt homogenization by intergranular diffusion mechanisms. In other words, low cell numbers indicate efficient interstitial dispersion of the elements and isotopic signatures whereas high cell numbers indicate inefficient dispersion. This effect is shown in Fig. 7a, where the results of plate modelling applied to $^{143}Nd/^{144}Nd$ isotope variations in the wall-rock are shown for variable cell numbers. This indicates that high cell numbers (i.e. 100 and 1000) result in steeper chromatographic fronts than low cell numbers (i.e. 10 and 20). The data best fit a model involving 20 cells. If the distance of melt infiltration was around 1 m, the critical distance of interstitial melt homogenization by intergranular diffusion would be about 5 cm. This should be treated as a rough estimate because intergranular diffusion is likely to be more efficient close to the dyke (i.e. amphibole peridotite) than further in the host (i.e. anhydrous peridotite). The probable cause of such features is the existence of a thermal

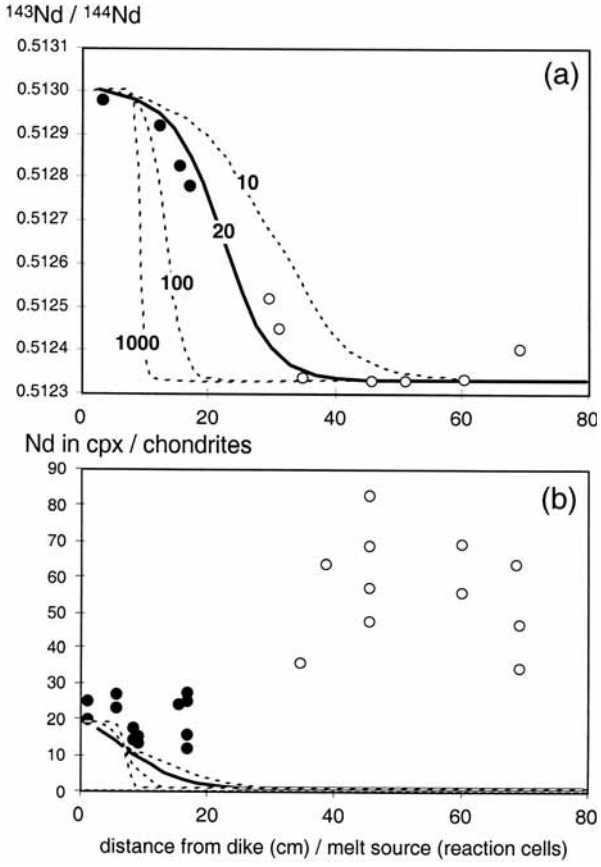

Fig. 7. Application of the 'plate model' (Vernières *et al.*, 1997) without reaction to the Nd isotopic variation in the wall-rock. In this approach, melt transport is not considered as a function of time and distance but simulated by propagation of melt batches through macrovolumes of mantle rock. The method assumes instantaneous mineral/melt equilibration as the melt batches move from one matrix cell to another and therefore, by comparison with the 1D models, disregards melt velocity, time and distance. To compare with analytical data, the plate model columns were arbitrarily scaled from 0 (bottom) to 80 (top). (a) Best fit of the Nd isotopic variation in the wall-rock (bold continuous line). The observed $^{143}Nd/^{144}Nd$ variation is best explained with a column of 20 cells, a porosity (melt fraction) of 0·2% and the presence of 4% modal amphibole in the peridotite. The compositional parameters (anhydrous protolith mineralogy and Nd content—$^{143}Nd/^{144}Nd$ ratio in melt and peridotite protolith) are the same as in the 1D model (Fig. 5). The dashed lines show the effect of modifying the number of cells in the model (10–1000, with no change of the other parameters) to improve the fit of Nd concentrations in clinopyroxene [shown in (b)]. (b) Bold continuous line shows Nd content in clinopyroxene calculated with the plate model and the set of parameters selected to fit the $^{143}Nd/^{144}Nd$ variation [shown in (a)]. The ion microprobe data obtained for clinopyroxene are shown for comparison. Dashed lines show results obtained by modifying the number of cells in the model to increase the Nd content in clinopyroxene while trying to keep the $^{143}Nd/^{144}Nd$ variation consistent with the measured values [shown in (a)].

and porosity gradient. This was proposed by Bodinier *et al.* (1990) on the basis of major-element gradients (higher Al, Ca and Fe) in the amphibole peridotite.

Similar to the 1D approach, plate modelling without reaction does not account for the abundances of Nd observed in the wall-rock (Fig. 7b). Near the dyke (i.e. magma source), the calculated Nd contents in cpx are somewhat higher than obtained with the 'best-fit' 1D model. However, when no reaction is involved the plate model is no better than the 1D model in accounting for Nd variation in the wall-rock, especially in the distal anhydrous peridotite.

Logically the next step in modelling was to precipitate amphibole. The precipitation of cpx is ignored for simplicity, the effect of this mineral on Nd variations being basically the same as that of amphibole. In the model, amphibole precipitation was allowed to occur in the lower quarter of the percolation column, adjacent to the magma source (= dyke). This is consistent with the observation that amphibole and secondary cpx are restricted to the amphibole peridotite (< 25 cm from the dyke). Based on textural observations indicating that amphibole occurs both in thin veinlets and as a replacive mineral after opx (Woodland *et al.*, 1996), the amphibole is formed in the model at the expense of both interstitial melt and opx. Whereas subtle differences in the input parameters (e.g. the rate of amphibole precipitation, i.e. the amount of amphibole precipitated relative to the amount of melt infiltrated) account for the different results (Fig. 8), all the models result in amphibole fractions varying from 4–5% close to the melt source to zero at some distance from the dyke, within the wall-rock (Fig. 8a). The average proportion of amphibole in the lower quarter of the column (1–2%) is consistent with the values actually observed in the amphibole harzburgite (leaving out the main lherzite veins). Most importantly, the models account reasonably well for the abrupt variation in $^{143}Nd/^{144}Nd$, the abundance of Nd, and the existence of two domains in the wall-rock, bounded by the reaction front of amphibole precipitation.

ALTERNATIVE HYPOTHESES

The model above assumes distinct origins for chemical (LREE) and isotopic (Sr–Nd) enrichment in the anhydrous harzburgite. The chemical enrichment is considered to be young, being related to dyke emplacement in the Cretaceous, whereas the isotopic enrichment would be much older, possibly linked to the harzburgite formation. An alternative to this model would be to ascribe the LREE enrichment to an early metasomatic stage. This scenario assumes a diffuse metasomatic event around 1000 Myr ago that would also account for modal (apatite), chemical and isotopic enrichment in the wall-rock protolith. Although rather unlikely—because strong LREE enrichment as observed in the studied wall-rock is not observed in harzburgites spatially unrelated to dykes—this model cannot be completely ruled out. Therefore, the hypothesis that the wall-rock was enriched in LREE before dyke injection must be examined. An

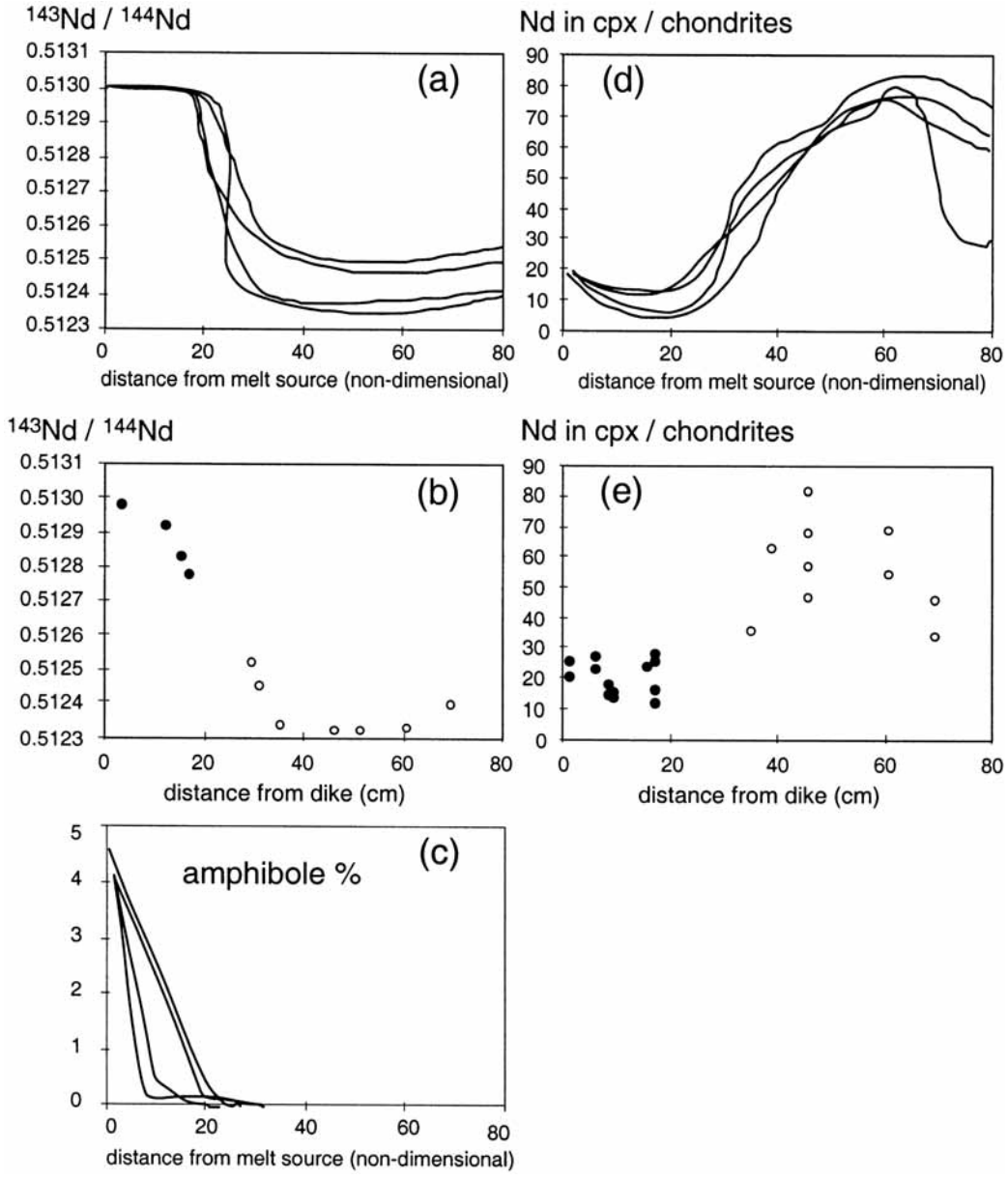

Fig. 8. Application of the 'plate model' (Vernières *et al.*, 1997) involving an amphibole-forming melt–rock reaction in the lower quarter of the percolation column. Amphibole precipitates at the expense of melt and pyroxene. Left: calculated $^{143}Nd/^{144}Nd$ variation (a) compared with the wall-rock analytical data (b). Four simulations are shown for variable amphibole precipitation and/or melt-consuming rates. The variation of the amphibole proportion is shown in (c). The initial conditions involve no amphibole in the wall-rock harzburgite protolith and a melt fraction of 1%. The compositional parameters (protolith mode, and Nd content and $^{143}Nd/^{144}Nd$ ratio in melt and protolith) are the same as in the other models (Fig. 5 caption). Because the melt fraction decreases as a result of the melt-consuming reaction, the cell volumes also decrease with distance from the melt source (Vernières *et al.*, 1997). Therefore, to compare with analytical data the results were first recast as constant-volume units before scaling the percolation columns between 0 and 80. Right: calculated Nd content in clinopyroxene (d) compared with the wall-rock SIMS data (e).

important implication of this scenario is the requirement that LREE and other highly incompatible elements (P) were 'drained' from the wall-rock into the dyke to account for the decreasing abundance of these elements toward the dyke. This can be achieved by the following processes.

(1) Advective element transport into partial melt tapped from the wall-rock by the dyke

Heating by melt flowing in the dyke could have triggered incipient melting of the wall-rock and migration of small fractions of partial melt into the fracture–vein system.

However, assuming a wall-rock protolith composition with $^{143}Nd/^{144}Nd = 0{\cdot}5124$, any melts generated within that protolith would have an identical ratio and migration of such melts toward the dyke would impart this isotopic composition on the wall-rock. This prediction is at variance with the systematic increase in $^{143}Nd/^{144}Nd$ observed from the enriched wall-rock toward the dyke. In addition, melting of the wall-rock could not explain the Fe-rich halo adjacent to the dyke, nor the overall fertile character of the amphibole harzburgite, compared with the anhydrous peridotite (i.e. the Al, Ca, Ti and HREE enrichment coupled with the presence of secondary cpx and amphibole).

(2) Diffusional transport via interstitial melt infiltrated from the dyke into the wall-rock

In this model, melt infiltration would explain Fe-enrichment and fertilization in the amphibole harzburgite, whereas interstitial diffusion in infiltrated melt would account for variable degrees of re-equilibration of the ultra-enriched wall-rock protolith to the less enriched compositions in equilibrium with melt in the dyke. Bodinier *et al.* (1990) suggested that intergranular diffusion via infiltrated melt might have been significant in the amphibole harzburgite (<25 cm), being enhanced by the thermal gradient and a high melt fraction. However, phosphorus shows a steadily increasing abundance much beyond the amphibole harzburgite zone, at a distance ≥ 75 cm from the dyke; this extended gradient of P is difficult to explain by diffusion (Fig. 1). Moreover, diffusion cannot explain the negative HFSE anomalies that occur in a transition zone (25–60 cm from the dyke) between amphibole harzburgite and the most distal apatite-bearing harzburgite, which both contain HFSE-undepleted cpx (Fig. 3).

(3) A combination of these two mechanisms: diffusion in infiltrated melt (amphibole harzburgite) and draining of incipient partial melt (apatite harzburgite)

A scenario involving diffusion in the infiltrated melt close to the dyke and draining of incipient melt further in the host might be envisioned to explain both the fertilization of the amphibole harzburgite, and the trace-element and isotopic variability in the wall-rock. However, even such a complex model would leave unexplained the negative HFSE anomalies in cpx at 25–60 cm from the dyke. On the other hand, these anomalies can be accounted for by a reactive porous flow model. They were interpreted by Bedini *et al.* (1997) and Ionov *et al.* (2002*a*) as 'transient' (chromatographic) signatures resulting from the precipitation of Nb-rich microphases (Ti-oxides or amphibole) along with melt percolation. Alternatively, these anomalies may be explained by the lower solubility of these elements in carbonate-rich derivatives of the infiltrated melt.

CONCLUSIONS

Reactive chromatograhic processes offer an explanation for the juxtaposition of the amphibole–garnet pyroxenite dyke, subordinate hornblendite veins, the amphibole harzburgite and the apatite-bearing harzburgite with a single-stage process. Both the amphibole and the apatite-forming metasomatic processes originated from the same dyke, which produced water-rich and carbonate-rich melts as derivatives from crystal segregation in a magma conduit (pyroxene–garnet in the dyke) and wall-rock reactions (amphibole $\pm$ cpx $\pm$ phlogopite in veins and wall-rock proximal to the dyke). In this particular example there is no necessity to invoke different and genetically distinct metasomatic melts or fluids (i.e. a hydrous silicate melt and a carbonate melt).

Modelling resolves the paradox of the spatial decoupling between isotopic contamination and LREE enrichment. Indeed, the simulation of isotopic variations during reactive porous flow confirms that the isotopic contamination (e.g. $^{143}Nd/^{144}Nd$) by the infiltrated melt is restricted to the domain between the melt source (= dyke) and the chromatographic front of the element (Nd), i.e. about 20 cm from the dyke in the studied wall-rock. However, the infiltration of small-volume melts probably occurred on a significantly greater distance in the host peridotite, as attested by the systematic increase in Th, U, LREE and P_2O_5, which reach a maximum in the apatite-bearing harzburgite wall-rock (>50 cm from the dyke). This indicates that small-volume melts have a limited capacity to modify the Nd–Sr isotopic composition of mantle rocks. The strong enrichment observed for Th, U, LREE and P_2O_5 in the distal wall-rock is ascribed to partial crystallization of the infiltrated melt as a result of amphibole $\pm$ cpx precipitation in the amphibole harzburgite reaction zone (<25 cm from the dyke). On the other hand, the negative anomalies observed for Ba and the HFSE (Nb, Ta, Zr and Hf) may result from the precipitation of very small amounts of phlogopite, and Ti- and Zr-oxides. Alternatively, the HFSE anomalies may also be explained by the lower solubility of these elements in the carbonate-rich derivatives of the infiltrated melt.

Whereas the trace-element variability in the wall-rock is best explained with a single-stage mechanism, the isotopic enrichment observed in the wall-rock at >30 cm from the dyke requires time-integration of LREE enrichment over $\sim$1000 Myr. This enrichment is inherited

from the wall-rock harzburgite protolith and probably linked to the formation or petrogenesis of the tabular harzburgites in Lherz. This enrichment is separated in time and space from crack propagation–melt injection, which occurred in the Cretaceous (~100 Ma), and led to melt infiltration, chromatographic fractionation and reaction, and the formation of amphibole and apatite.

A probable chronology of events follows, with (1) being separated in time and space from (2)–(4), which are essentially synchronous.

(1) Formation of the enriched harzburgite wall-protolith, probably linked to the petrogenesis of the tabular harzburgites in Lherz, which occurred well before emplacement of the dykes or veins (Fabriès *et al.*, 1991; Reisberg & Lorand, 1995; Bodinier & Godard, ~~2004~~).

(2) Emplacement of a 'trans-lithospheric' complex of feeder dykes for the alkaline basalts associated with lithospheric thinning in the northern Pyrenees zone during the Cretaceous (~100 Ma), only a few million years before the exhumation of the peridotite bodies in the North Pyrenean basins (Fabriès *et al.*, 1991, 1998). The slight change in texture from 'sheared' (proximal to the dyke) to 'less sheared/granular' (distal to the dyke) records wall-rock deformation during or soon after dyke injection.

(3) Crystal segregation of pyroxene and garnet in the dyke conduits, associated with concomitant release of hydrous melts, which resulted in fluid-assisted fracturing of the wall-rock and crystallization of lherzites in branching and anastomosing veins. This was accompanied by more diffuse, intergranular percolation of melt in the dyke and the proximal wall-rock, which led to the formation of poikiloblastic amphibole in the dyke and the precipitation of secondary amphibole (±cpx) in the amphibole harzburgite zone (< 25 cm from the dyke).

(4) Amphibole ± cpx crystallization, resulting in further evolution of the residual melt and producing a carbonate-rich melt that was strongly enriched in P, LREE and Th–U. The carbonate melt migrated beyond the amphibole-forming reaction front and precipitated apatite in the distal wall-rock (> 25 cm). The fact that several incompatible elements have their chromatographic fronts near coincident with the transition between the amphibole-forming reaction front (i.e. in the range 20–30 cm) suggests that the front corresponds to a significant drop in melt/rock ratio. The amphibole harzburgite reaction zone was probably bounded by a thermally controlled, permeability barrier along which hydrous silicate melts were refracted. The boundary was nevertheless traversed by low-T, carbonated small melt fractions. In that sense, the proximal amphibole peridotite may be considered as a small-scale analogue of the thermal boundary layer, at the base of lithospheric mantle infiltrated by plume-derived melts (Bedini *et al.*, 1997; Baker *et al.*, 1998; Xu *et al.*, 1998).

ACKNOWLEDGEMENTS

We acknowledge the collaborative efforts of Gilles Bussod and Alan Woodland during the early stages of this project. Elaine MacPherson was supported by an NERC studentship at Royal Holloway. Matthew Thirlwall is thanked for his co-supervision of Elaine and for the provision of high-quality isotope data. However, this paper would not have been possible without the considerable talent and efforts of Jacques Vernières and his success in modelling isotopes during chromatographic processes. We thank Ben Harte, Masaaki Obata and an anonymous reviewer for their comments that improved the manuscript. We dedicate this paper to our late colleague, Professor Jacques Fabriès, who promoted recent research on mantle metasomatism in Lherz and, in particular, selected the wall-rock for the present study.

REFERENCES

Baker, J. B., Chazot, G., Menzies, M. A. & Thirlwall, M. F. (1998). Metasomatism of the shallow mantle beneath Yemen by the Afar plume—implications for mantle plumes, flood volcanism and intraplate volcanism. *Geology* **26**, 431–434.

Bedini, R. M., Bodinier, J.-L., Dautria, J.-M. & Morten, L. (1997). Evolution of LILE-enriched small melt fractions in the lithospheric mantle: a case study from the East African Rift. *Earth and Planetary Science Letters* **153**, 67–83.

Bodinier, J.-L. & Godard, M. (~~2004~~). Orogenic, ophiolitic and abyssal peridotites. In: Carlson, R. W. (ed.) *Volume 2: Geochemistry of the Mantle and Core*. In: Turekian, K. & Holland, H. (eds) *Treatise on Geochemistry*, in press.

Bodinier, J.-L., Fabriès, J., Lorand, J.-P., Dostal, J. & Dupuy, C. (1987*a*). Geochemistry of amphibole pyroxenite veins from the Lherz and Freychinède ultramafic bodies (Ariège, French Pyrénées). *Bulletin de Minéralogie* **110**, 345–358.

Bodinier, J.-L., Guiraud, M., Fabriès, J., Dostal, J. & Dupuy, C. (1987*b*). Petrogenesis of layered pyroxenites from the Lherz, Freychinède and Prades ultramafic bodies (Ariège, French Pyrénées). *Geochimica et Cosmochimica Acta* **51**, 279–290.

Bodinier, J.-L., Dupuy, C. & Dostal, J. (1988). Geochemistry and petrogenesis of eastern Pyrenean peridotites. *Geochimica et Cosmochimica Acta* **52**, 2893–2907.

Bodinier, J.-L., Vasseur, G., Vernières, J., Dupuy, C. & Fabriès, J. (1990). Mechanisms of mantle metasomatism: geochemical evidence from the Lherz orogenic peridotite. *Journal of Petrology* **31**, 597–628.

Burnham, O. M., Rogers, N. W., Pearson, D. G., van Calsteren, P. W. & Hawkesworth, C. J. (1998). The petrogenesis of the eastern Pyrenean peridotites: an integrated study of their whole-rock geochemistry and Re–Os isotope composition. *Geochimica et Cosmochimica Acta* **62**, 2293–2310.

Dautria, J.-M., Dupuy, C., Takherist, D. & Dostal, J. (1992). Carbonate metasomatism in the lithospheric mantle: xenoliths from a melilitic district of the Sahara basin. *Contributions to Mineralogy and Petrology* **111**, 37–52.

De Marsily, G. (1986). *Quantitative Hydrogeology. Groundwater Hydrology for Engineers*. London: Academic Press, 440 pp.

Downes, H., Bodinier, J.-L., Thirlwall, M. F., Lorand, J.-P. & Fabriès, J. (1991). REE and Sr–Nd isotopic geochemistry of Eastern

Pyrenean peridotites massifs: sub-continental lithospheric mantle modified by continental magmatism. *Journal of Petrology, Special Lherzolite Issue* 97–115.

Downes, H., Embey-Isztin, A. & Thirlwall, M. F. (1992). Petrology and geochemistry of spinel peridotite xenoliths from the western Panonian Basin (Hungary): evidence for an association between enrichment and texture in the upper mantle. *Contributions to Mineralogy and Petrology* **109**, 340–354.

Fabriès, J., Lorand, J.-P., Bodinier, J.-L. & Dupuy, C. (1991). Evolution of the upper mantle beneath the Pyrenees: evidence from orogenic spinel lherzolite massifs. *Journal of Petrology, Special Lherzolite Issue* 55–76.

Fabriès, J., Lorand, J.-P. & Bodinier, J.-L. (1998). Petrogenetic evolution of orogenic lherzolite massifs in the central and western Pyrenees. *Tectonophysics* **292**, 145–167.

Godard, M., Bodinier, J.-L. & Vasseur, G. (1995). Effects of mineralogical reactions on trace element redistributions in mantle rocks during percolation processes: a chromatographic approach. *Earth and Planetary Science Letters* **133**, 449–461.

Godard, M., Jousselin, D. & Bodinier, J.-L. (2000). Relationships between geochemistry and structure beneath a paleo-ridge centre: a study of the mantle section in the Oman ophiolite. *Earth and Planetary Science Letters* **180**, 133–148.

Goldberg, G. M., Maluski, H. & Leyreloup, A. F. (1986). Petrological and age relationship between emplacement of magmatic breccia, alkaline magmatism and static metamorphism in the North Pyrenean Zone. *Tectonophysics* **129**, 275–290.

Hamelin, B. & Allègre, C. J. (1988). Lead isotope study of orogenic lherzolite massifs. *Earth and Planetary Science Letters* **91**, 117–131.

Hart, S. R. & Dunn, T. (1993). Experimental cpx/melt partitioning of 24 trace elements. *Contributions to Mineralogy and Petrology* **113**, 1–8.

Harte, B., Hunter, R. H. & Kinny, P. D. (1993). Melt geometry, movement and crystallization, in relation to mantle dykes, veins and metasomatism. *Philosophical Transactions of the Royal Society of London, Series A* **342**, 1–21.

Hauri, E. K., Shimizu, N., Dieu, J. J. & Hart, S. R. (1993). Evidence for hotspot related carbonatite metasomatism in the oceanic upper mantle. *Nature* **365**, 221–227.

Ionov, D. A. & Hofmann, A. W. (1995). Nb–Ta-rich mantle amphiboles and micas: implications for subduction-related metasomatic trace element fractionations. *Earth and Planetary Science Letters* **198**, 495–510.

Ionov, D. A., Savoyant, L. & Dupuy, C. (1992). Application of the ICP-MS technique to trace-element analysis of peridotites and their minerals. *Geostandards Newsletter* **16**, 311–315.

Ionov, D. A., Dupuy, C., O'Reilly, S. Y., Kopylova, M. G. & Genshaft, Y. S. (1993). Carbonated peridotite xenoliths from Spitsbergen: implications for trace element signature of mantle carbonate metasomatism. *Earth and Planetary Science Letters* **119**, 283–297.

Ionov, D. A., Bodinier, J.-L., Mukasa, S. B. & Zanetti, A. (2002*a*). Mechanisms and sources of mantle metasomatism: major and trace element compositions of peridotite xenoliths from Spitsbergen in the context of numerical modeling. *Journal of Petrology* **43**, 2219–2259.

Ionov, D. A., Mukasa, S. B. & Bodinier, J.-L. (2002*b*). Sr–Nd–Pb Isotopic compositions of peridotite xenoliths from Spitsbergen: numerical modeling indicates Sr–Nd decoupling in the mantle by melt percolation metasomatism. *Journal of Petrology* **43**, 2261–2278.

Kelemen, P. B., Shimizu, N. & Dunn, T. (1993). Relative depletion of niobium in some arc magmas and the continental crust; partitioning of K, Nb, La and Ce during melt/rock reaction in the upper mantle. *Earth and Planetary Science Letters* **120**, 111–133.

Lorand, J.-P., Gros, M. & Pattou, L. (1999). Fractionation of platinum-group element in the upper mantle: a detailed study in Pyrenean orogenic peridotites. *Journal of Petrology* **40**, 951–987.

Loubet, M. & Allègre, C. J. (1982). Trace elements in orogenic lherzolites reveal the complex history of the upper mantle. *Nature* **298**, 809–814.

McPherson, E. (1994). Geochemistry of silicate melt metasomatism in alpine peridotite massifs. Ph.D. thesis, University of London.

McPherson, E., Thirlwall, M. F., Parkinson, I. J., Menzies, M. A., Bodinier, J.-L., Woodland, A. & Bussod, G. (1996). Geochemistry of metasomatism adjacent to amphibole-bearing veins in the Lherz peridotite massif. *Chemical Geology* **131**, 135–157.

Menzies, M. A., Rogers, N., Tindle, A. & Hawkesworth, C. J. (1987). Metasomatic enrichment processes in lithospheric peridotites, an effect of asthenosphere–lithosphere interaction. In: Menzies, M. A. & Hawkesworth, C. J. (eds) *Mantle Metasomatism*. London: Academic Press, pp. 313–361.

Mukasa, S. B., Shervais, J. W., Wilshire, H. G. & Nielson, J. (1991). Intrinsic Nd, Pb and Sr isotopic heterogeneities exhibited by the Lherz alpine peridotite massif, French Pyrenees. *Journal of Petrology, Special Lherzolite Issue* 117–134.

Navon, O. & Stolper, E. (1987). Geochemical consequence of melt percolation: the upper mantle as a chromatographic column. *Journal of Geology* **95**, 285–307.

Nielson, J. E. & Wilshire, H. G. (1993). Magma transport and metasomatism in the mantle: a critical review of current geochemical models. *American Mineralogist* **78**, 1117–1134.

Pattou, L., Lorand, J.-P. & Gros, M. (1996). Non-chondritic PGE ratios in the terrestrial upper mantle. *Nature* **379**, 712–715.

Polvé, M. & Allègre, C. J. (1980). Orogenic lherzolite complexes studied by ^{87}Rb–^{87}Sr: a clue to understand the mantle convection processes? *Earth and Planetary Science Letters* **51**, 71–93.

Reisberg, L. & Lorand, J.-P. (1995). Longevity of sub-continental mantle lithosphere from osmium isotope systematics in orogenic peridotite massifs. *Nature* **376**, 159–162.

Rossy, M., Azambre, B. & Albarède, F. (1992). REE and Sr–Nd isotope geochemistry of the alkaline magmatism from the Cretaceous North Pyrenean Rift Zone (France–Spain). *Chemical Geology* **97**, 33–46.

Rudnick, R. L., McDonough, W. F. & Chappel, B. W. (1993). Carbonatite metasomatism in the northern Tanzanian mantle: petrographic and geochemical characteristics. *Earth and Planetary Science Letters* **114**, 463–475.

Shimizu, N. & Hart, S. R. (1982). Application of the ion microprobe to geochemistry and cosmochemistry. *Annual Review of Earth and Planetary Sciences* **10**, 483–526.

Sun, S. S. & McDonough, W. F. (1989). Chemical and isotopic systematics of oceanic basalts: implications for mantle composition and processes. In: Saunders, A. D. & Norry, M. J. (eds) *Magmatism in the Ocean Basins. Geological Society, London, Special Publications* **42**, 313–345.

Takazawa, E., Frey, F. A., Shimizu, N. & Obata, M. (1996). Evolution of the Horoman peridotite (Hokkaido, Japan): implications from pyroxene compositions. *Chemical Geology* **134**, 3–26.

Thirlwall, M. F. (1982). A triple filament method for rapid and precise analysis of rare earth elements by isotope dilution. *Chemical Geology* **35**, 155–166.

Thirlwall, M. F. (1991). Long-term reproducibility of mulicollector Sr and Nd isotope ratio analysis. *Chemical Geology* **94**, 85–104.

Tiepolo, M., Bottazzi, P., Foley, S. Oberti, R., Vannucci, R. & Zanetti, A. (2001). Fractionation of Nb and Ta from Zr and Hf at mantle depths: the role of titanian pargasite and kaersutite. *Journal of Petrology* **42**, 221–232.

Vasseur, G., Vernières, J. & Bodinier, J.-L. (1991). Modelling of trace-element transfer between mantle melt and heterogranular peridotite matrix. *Journal of Petrology, Special Lherzolite Issue* 41–54.

Vernières, J., Godard, M. & Bodinier, J.-L. (1997). A plate model for the simulation of trace element fractionation during partial melting and magma transport in the Earth's upper mantle. *Journal of Geophysical Research* **102**, 24771–24784.

Vétil, J.-Y., Lorand, J.-P. & Fabriès, J. (1988). Conditions de mise en place des filons de pyroxénites à amphibole du massif ultramafique de Lherz (Ariège, France). *Comptes Rendus de l'Académie des Sciences* **307**, 587–593.

Wilshire, H. G., Pike, J. E. N., Meyer, C. E. & Schwarzmann, E. L. (1980). Amphibole-rich veins in lherzolite xenoliths, Dish Hill and Deadman Lake, California. *American Journal of Science* **280A**, 576–593.

Witt-Eickschen, G. & Harte, B. (1994). Distribution of trace elements between amphibole and clinopyroxene from mantle peridotites of the Eifel (western Germany); an ion-microprobe study. *Chemical Geology* **117**, 235–260.

Woodland, A. B., Kornprobst J., McPherson, E., Bodinier, J.-L. & Menzies, M. A. (1996). Metasomatic interactions in the lithospheric mantle: petrologic evidence from the Lherz massif, French Pyrenees. *Chemical Geology* **134**, 83–112.

Xu, Y.-G., Menzies, M. A., Bodinier, J.-L., Bedini, R. M., Vroon, P. & Mercier, J.-C. C. (1998). Melt percolation-reaction at the lithosphere–plume boundary: evidence from the poikiloblastic peridotite xenoliths from Borée (Massif Central, France). *Contributions to Mineralogy and Petrology* **132**, 65–84.

Zanetti, A., Vannucci, R., Bottazzi, P., Oberti, R. & Ottolini, L. (1996). Infiltration metasomatism at Lherz as monitored by systematic ion-microprobe investigations close to a hornblendite vein. *Chemical Geology* **134**, 113–133.

Zangana, N. A., Downes, H., Thirlwall, M. F. & Hegner, L. (1997). Relationship between deformation, equilibration temperatures, REE and radiogenic isotopes in mantle xenoliths (Ray Pic, Massif Central, France): an example of plume–lithosphere interaction? *Contributions to Mineralogy and Petrology* **127**, 187–203.